

Higgs flavor phenomenology in a supersymmetric left-right model with parity

Syuhei Iguro¹, Junichiro Kawamura^{2,3}, Yuji Omura⁴, and Yoshihiro Shigekami⁵

¹*Department of Physics, Nagoya University, Chikusa-ku, Nagoya 464-8602, Japan*

²*Center for Theoretical Physics of the Universe, Institute for Basic Science (IBS), Yuseong-gu, Daejeon 34126 Korea*

³*Department of Physics, Keio University, Kohoku-ku, Yokohama 223-8522, Japan*

⁴*Department of Physics, Kindai University, Higashi-Osaka, Osaka 577-8502, Japan*

⁵*School of Physics, Huazhong University of Science and Technology, Luoyu Road 1037, Wuhan 430074, China*

Abstract

In this paper, we focus on the supersymmetric model with left-right (LR) symmetry, that is especially proposed in our previous work [1]. In this model, there are four Higgs doublets in order to realize the Standard Model (SM) fermion masses and the Cabibbo-Kobayashi-Maskawa matrix. The heavy Higgs doublets unavoidably have flavor changing couplings to the SM fermions and induce flavor-changing neutral currents at tree level. We study broader parameter space than the previous work with including the renormalization group corrections to the Yukawa couplings between the LR breaking scale, $\mathcal{O}(10^{13})$ GeV, and the supersymmetry breaking scales, $\mathcal{O}(100)$ TeV. The CP violating observable in K - \bar{K} mixing, ϵ_K , strongly constrains the model, so that heavy Higgs mass should be heavier than $\mathcal{O}(100)$ TeV. We study the lepton flavor violating (LFV) processes setting heavy Higgs masses to be 170 TeV. The branching ratios of $\mu \rightarrow 3e$ and the μ - e conversion can be larger than 10^{-16} that could be covered by the future experiments. We also study the degree of fine-tuning in the parameter region that predicts testable LFV processes.

Contents

1	Introduction	2
2	The LR symmetric model with SUSY	3
3	RG effects to Yukawa couplings	5
3.1	RG equations above the SUSY breaking scale	6
3.2	The SM fermion masses	7
3.3	Parametrization and outline of numerical analysis	8
4	Flavor physics induced by heavy Higgs	10
4.1	$\Delta F = 2$ processes	10
4.2	LFV processes	13
4.3	Leptonic meson decays	19
5	Summary	21
A	Details of the scan	22
A.1	Fitting and scanning	22
A.2	Benchmark	23

1 Introduction

The Standard Model (SM) of elementary particle physics has succeeded in explaining most of the experimental results so far. The SM, however, needs to be extended to solve the theoretical problems, e.g. the strong CP problem and the gauge hierarchy problem. In Ref. [1], three of the authors have studied the model with the left-right (LR) symmetry [2, 3] and supersymmetry (SUSY) [4, 5], where the LR symmetry, that is kind of parity, is broken at the intermediate scale, $\mathcal{O}(10^{10})$ GeV. Hence, the strong CP problem could be solved [6, 7]¹. Besides, the gauge hierarchy problem is solved by SUSY, although there still remains the little hierarchy problem to explain the electroweak (EW) scale when the SUSY breaking scale resides at $\mathcal{O}(100)$ TeV to explain the observed Higgs boson mass [13–16]. Another advantage of SUSY would be the naturalness of the hierarchy between the LR and EW symmetry breaking scales. The former is realized in SUSY conserving potential, while the latter is induced by the SUSY breaking effects as will be shown explicitly later².

In the LR symmetric model with SUSY, at least two Higgs bi-doublets should be introduced to realize the realistic Yukawa couplings at the renormalizable level. One mode of the four Higgs doublets from two bi-doublets is identified as the SM Higgs boson whose mass is measured at 125 GeV [18, 19]. The other doublets may reside around the SUSY breaking scale depending on mediation mechanisms of the SUSY breaking. Those Higgs bosons will induce flavor changing neutral currents (FCNCs) at the tree level, as well as signals at the collider experiments [20–33]. If two of four Higgs doublets are light, the model corresponds to a generic two Higgs doublet model (2HDM). Unlike the conventional minimal supersymmetric SM, one Higgs doublet effectively couples to both up-type and down-type quarks, and hence that will induce tree-level FCNCs. Such a general 2HDM is widely discussed to explain the recent flavor anomalies [34–55].

In this paper, we update the analysis of the model studied in Ref. [1]. An important progress in this work is that the LR breaking effects via renormalization group (RG) running are explicitly taken into account. The effects is expected to be quantitatively significant since the LR symmetry breaking scale is very far from the SUSY breaking scale and some couplings are close to be $\mathcal{O}(1)$. Another progress is that we scan over wider parameter space in more systematic way. We numerically study the allowed parameter region that is consistent with both the LR symmetry and the SM fermion mass matrices.

With the LR symmetry, the Yukawa matrices are hermitian and are universal for up- and down-type fermions. After the LR symmetry breaking, the splitting of the Yukawa matrices is given by the linear combination of two Yukawa couplings to the bi-doublets. In the analysis, we scan over parameter space that is consistent with the hermitian and universal Yukawa couplings at the LR symmetry breaking scale and reproduces the re-

¹See also recent discussions [8–12].

²The LR breaking effects from SUSY breaking should be sufficiently suppressed to solve the strong CP [17].

	Q_L^i	\hat{Q}_R^{ci}	\hat{L}_L^i	\hat{L}_R^{ci}	Φ_a	Δ_L	$\bar{\Delta}_L$	Δ_R	$\bar{\Delta}_R$	S
$SU(3)_C$	3	$\bar{\mathbf{3}}$	1	1	1	1	1	1	1	1
$SU(2)_L$	2	1	2	1	2	3	3	1	1	1
$SU(2)_R$	1	2	1	2	2	1	1	3	3	1
$U(1)_{B-L}$	1/3	-1/3	-1	1	0	2	-2	-2	2	0

Table 1: Matter contents of the LR symmetric model with SUSY. $i, j = 1, 2, 3$ are the flavor indices for the quarks and leptons, and $a, b = 1, 2$ are the indices for the bi-doublet fields, $\Phi_{1,2}$.

alistic fermion masses and the Cabibbo-Kobayashi-Maskawa (CKM) matrix at the EW scale. We find explicit predictions of FCNCs, and discuss the sensitivities of our model at the future experiments.

This paper is organized as follows. In section 2, we briefly review the model discussed in Ref. [1]. In section 3, we show the RG equations that give the connection between the LR breaking scale and the SUSY scale. Section 4 is devoted to the low energy flavor phenomenology of the scalar sector of the LR SUSY model. The summary of the paper is given in section 5. In the appendix A, we explain the detail of the fit procedure to find the model parameters that realize the realistic fermion masses and the CKM matrix.

2 The LR symmetric model with SUSY

We shall briefly introduce the model proposed in Ref. [1]. The model respects not only SUSY but also the LR symmetry. The matter contents of the model is summarized in Table 1. We decompose the superpotential as

$$W = W_{\text{vis}} + W_{\text{SB}} + W_{\Delta_L}, \quad (1)$$

where W_{vis} is for the visible sector, W_{SB} is for the $SU(2)_R$ breaking and W_{Δ_L} is for preserving the LR symmetry. We introduce two bi-doublet fields, Φ_a ($a = 1, 2$), in order to realize the realistic Yukawa coupling. The superpotential of the visible sector is given by

$$W_{\text{vis}} = Y_{ij}^a \hat{Q}_L^i \tau_2 \Phi_a \tau_2 \hat{Q}_R^{cj} + Y_{ij}^{\ell a} \hat{L}_L^i \tau_2 \Phi_a \tau_2 \hat{L}_R^{cj} + \frac{1}{2} \lambda_{ij}^\nu \hat{L}_R^{ci} \Delta_R \tau_2 \hat{L}_R^{cj} + \frac{1}{2} \mu^{ab} \text{Tr} (\tau_2 \Phi_a^T \tau_2 \Phi_b), \quad (2)$$

where $\tau_2 = i\sigma_2$ with the Pauli matrix σ_2 . The $SU(2)_L$ doublets are defined as $\hat{Q}_L^i = (\hat{u}_L^i, \hat{d}_L^i)$ and $\hat{L}_L^i = (\hat{n}_L^i, \hat{e}_L^i)$, and the $SU(2)_R$ doublets are defined as $\hat{Q}_R^{cj} = (\hat{d}_R^{cj}, -\hat{u}_R^{cj})$ and $\hat{L}_R^{cj} = (\hat{e}_R^{cj}, -\hat{n}_R^{cj})$. The third term generates the Majorana masses for the right-handed neutrinos \hat{n}_R^c via the non-zero VEV of Δ_R . The last term is the μ -term of the Higgs superfields. Note that μ^{ab} is 2×2 matrix since there are two bi-doublets. Following

our previous work [1], the hatted fields represent the basis in which the gauge interactions and μ -term are diagonalized, i.e. $\mu^{ab} = \mu^a \delta_{ab}$.

We consider a scenario in which Δ_R develops a large VEV, so that the Majorana mass term is induced at the intermediate scale for the type-I seesaw mechanism. The superpotential for the symmetry breaking, $SU(2)_R \times U(1)_{B-L} \rightarrow U(1)_Y$, is given by ³,

$$W_{\text{SB}} = m(S) \text{Tr} (\Delta_R \bar{\Delta}_R) + w(S), \quad (3)$$

where $m(S)$ and $w(S)$ are the holomorphic functions of the singlet field S . The F-terms of Δ_R , $\bar{\Delta}_R$ and S are respectively given by

$$-F_{\Delta_R}^\dagger = m(S) \bar{\Delta}_R, \quad -F_{\bar{\Delta}_R}^\dagger = m(S) \Delta_R, \quad -F_S^\dagger = \text{Tr} (\Delta_R \bar{\Delta}_R) \partial_S m(S) + \partial_S w(S), \quad (4)$$

and the D-terms are given by

$$D_{SU(2)_R}^A = 2 \text{Tr} (\Delta_R^\dagger \tau_R^A \Delta_R) + 2 \text{Tr} (\bar{\Delta}_R^\dagger \tau_R^A \bar{\Delta}_R), \quad (5)$$

$$D_{U(1)_{B-L}} = \xi - 2 \text{Tr} (\Delta_R^\dagger \Delta_R) \text{Tr} (\bar{\Delta}_R^\dagger \bar{\Delta}_R), \quad (6)$$

where $\tau_R^A = \sigma^A/2$ is the representation matrix for $SU(2)_R$ and $A = 1, 2, 3$. Here, we assume that the scalar partners of the SM fermions do not develop VEVs due to the positive soft mass squared. ξ is the FI-term for the $U(1)_{B-L}$. The symmetry breaking, $SU(2)_R \times U(1)_{B-L} \rightarrow U(1)_Y$, is realized if the vacuum is located at

$$\langle \Delta_R \rangle = \begin{pmatrix} 0 & 0 \\ v_R & 0 \end{pmatrix}, \quad \langle \bar{\Delta}_R \rangle = \begin{pmatrix} 0 & \bar{v}_R \\ 0 & 0 \end{pmatrix}. \quad (7)$$

In fact, this is one of the global minimum of the scalar potential where the SUSY breaking effects are negligible, i.e.

$$F_{\Delta_R}^\dagger, F_{\bar{\Delta}_R}^\dagger \propto m(S) = 0, \quad -F_S^\dagger = v_R \bar{v}_R \partial_S w(S) + \partial_S m(S) = 0, \quad (8)$$

and

$$D_{SU(2)_R}^{1,2} = 0, \quad D_{SU(2)_R}^3 = |v_R|^2 - |\bar{v}_R|^2 = 0, \quad D_{U(1)_{B-L}} = \xi - 2(|v_R|^2 - |\bar{v}_R|^2). \quad (9)$$

The D-term conditions are satisfied if $|v_R| = |\bar{v}_R|$ and $\xi = 0$. The values of $|v_R| = |\bar{v}_R|$ and $\langle S \rangle$ are fixed such that the F-term conditions in Eq. (8) are satisfied. Phenomenologically, the symmetry breaking scale should be at $\mathcal{O}(10^{13}\text{-}10^{14})$ GeV for the type-I seesaw mechanism. Note that for tiny neutrino masses, the LR breaking scale can be lower than 10^{14} GeV, as explained in e.g., Refs. [60–71]. In our analysis, the neutrino Yukawa couplings are assumed to be $\mathcal{O}(1)$, and therefore, we consider high-scale LR breaking throughout this paper. It is important that the bi-doublets Φ_a are not coupled with Δ_R due to

³This model has been proposed in Ref. [56], and the similar setups are discussed in Refs. [57–59].

$U(1)_{B-L}$ at the renormalizable level, and hence the Higgs doublets are free from the large VEVs of Δ_R and $\overline{\Delta}_R$ ⁴.

We introduce $SU(2)_L$ triplet fields, Δ_L and $\overline{\Delta}_L$, in order to make the model invariant under the LR exchanging transformation,

$$\hat{Q}_L \leftrightarrow \hat{Q}_R^{\dagger}, \quad \hat{L}_L \leftrightarrow \hat{L}_R^{\dagger}, \quad \Phi_a \leftrightarrow \Phi_a^{\dagger}, \quad \Delta_L \leftrightarrow \Delta_R^{\dagger}, \quad \overline{\Delta}_L \leftrightarrow \overline{\Delta}_R^{\dagger}, \quad S \leftrightarrow S^{\dagger}. \quad (10)$$

The Yukawa matrices for quarks are hermitian due to the LR symmetry ⁵, and hence the θ_{QCD} term would be sufficiently suppressed at the QCD scale. The superpotential involving those triplets are given by

$$W_{\Delta_L} = \{m_L + m(S)\} \text{Tr}(\Delta_L \overline{\Delta}_L) + \frac{1}{2} \lambda_{ij}^{\nu*} \hat{L}_L^i \tau_2 \Delta_L \hat{L}_L^j. \quad (11)$$

Here we introduce the soft LR symmetry breaking mass m_L , so that the triplets Δ_L and $\overline{\Delta}_L$ have SUSY mass terms at the SUSY vacuum with $\langle \Delta_L \rangle = \langle \overline{\Delta}_L \rangle = 0$. For instance, m_L can be generated by the term $W \supset \frac{1}{M_p} \text{Tr}(\Delta_L \overline{\Delta}_L) \text{Tr}(\Delta_R \overline{\Delta}_R)$ with M_p being the Planck mass, and then the size is estimated as $m_L = v_R^2/M_p \sim 10^{10}$ GeV when $v_R = 10^{14}$ GeV. The Majorana mass terms for left-handed neutrinos are absent at this vacuum. This soft breaking will be negligible compared with the spontaneous symmetry breaking by $v_R = \bar{v}_R \neq 0$. Note that θ_{QCD} is vanishing at tree level.

The bi-doublet fields are decomposed to the up- and down-type doublets, $\Phi_a = (-H_u^a, H_d^a)$ whose the hypercharges are respectively $+1/2$ and $-1/2$. The scalar potential of the Higgs doublets are given by

$$V_H = \{(m_{H_u}^2)_{ab} + |\mu^a|^2 \delta_{ab}\} H_u^{\dagger} H_u^b + \{(m_{H_d}^2)_{ab} + |\mu^a|^2 \delta_{ab}\} H_d^{\dagger} H_d^b + (B^{ab} H_d^a \tau_2 H_u^b + h.c.) + V_D, \quad (12)$$

where V_D is the D-term potential of the Higgs bosons. Here, $m_{H_u}^2$, $m_{H_d}^2$ and B are the soft SUSY breaking terms. These are, in general, 2×2 hermitian matrices. In the analysis, we assume that this potential has the global minimum which breaks the EW symmetry consistently with the observations. Note that $\mathcal{O}(10^6)$ tuning may be necessary to explain the EW scale if the soft SUSY breaking scale is at $\mathcal{O}(100 \text{ TeV})$ as considered in our analysis ⁶.

3 RG effects to Yukawa couplings

We evaluate the RG correction to the Yukawa couplings at the one-loop level. The LR symmetry breaking scale in the analysis is set to be $\mathcal{O}(10^{13}\text{-}10^{14})$ GeV, so that the

⁴We assume that the Higgs bi-doublets do not have large mass terms nor renormalizable coupling with S , so that the μ -terms are at the SUSY breaking scale. These would be prohibited by e.g. discrete R symmetry [72, 73].

⁵The symmetry also requires μ^{ab} to be real.

⁶The fine-tuning could be perhaps avoided if the SUSY breaking has an appropriate hierarchy, see e.g. Refs. [74–77].

correction may significantly change the Yukawa couplings. In our previous work [1], these are absorbed by the Higgs mixing parameters which can be done by exploiting the holomorphy of superpotential; see Appendix D of Ref. [1] for more details. In this work, we take closer look at the RG effects by solving RG equations (RGEs) numerically, and also the mixing among the Higgs bosons. We can see phenomenological consequences of the hermitian structure at the LR breaking scale explicitly.

3.1 RG equations above the SUSY breaking scale

After the LR symmetry is broken at the scale, $\mu_R := v_R$, the Yukawa couplings to the quarks and charged leptons are given by ⁷

$$-\mathcal{L}_{\text{yuk}} = -(Y_u^a)_{ij} H_u^a \tau_2 \hat{Q}_L^i \hat{u}_R^{c,j} + (Y_d^a)_{ij} H_d^a \tau_2 \hat{Q}_L^i \hat{d}_R^{c,j} + (Y_e^a)_{ij} H_d^a \tau_2 \hat{L}_L^i \hat{e}_R^{c,j} + h.c.. \quad (13)$$

The Yukawa couplings at $\mu = \mu_R$ are given by

$$Y_u^a(\mu_R) = Y_d^a(\mu_R) = Y^a, \quad Y_e^a(\mu_R) = Y^{\ell a}, \quad a = 1, 2, \quad (14)$$

where the flavor indices are omitted. The hermitian Yukawa matrices, Y^a and $Y^{\ell a}$, are defined in Eq. (2).

These six Yukawa matrices are evolved by the RGEs:

$$16\pi^2 \mu \frac{d}{d\mu} Y_u^a = \gamma_{H_u}^{ab} Y_u^b + Y_u^b Y_u^{b\dagger} Y_u^a + Y_d^b Y_d^{b\dagger} Y_u^a + 2Y_u^a Y_u^{b\dagger} Y_u^b - \left(\frac{16}{3} g_s^2 + 3g^2 + \frac{13}{9} g'^2 \right) Y_u^a, \quad (15)$$

$$16\pi^2 \mu \frac{d}{d\mu} Y_d^a = \gamma_{H_d}^{ab} Y_d^b + Y_u^b Y_u^{b\dagger} Y_d^a + Y_d^b Y_d^{b\dagger} Y_d^a + 2Y_d^a Y_d^{b\dagger} Y_d^b - \left(\frac{16}{3} g_s^2 + 3g^2 + \frac{7}{9} g'^2 \right) Y_d^a, \quad (16)$$

$$16\pi^2 \mu \frac{d}{d\mu} Y_e^a = \gamma_{H_d}^{ab} Y_e^b + Y_e^b Y_e^{b\dagger} Y_e^a + 2Y_e^a Y_e^{b\dagger} Y_e^b - (3g^2 + 3g'^2) Y_e^a, \quad (17)$$

where $\gamma_{H_u}^{ab}$ and $\gamma_{H_d}^{ab}$ are given by

$$\gamma_{H_u}^{ab} = 3 \text{Tr}(Y_u^a Y_u^{b\dagger}), \quad \gamma_{H_d}^{ab} = 3 \text{Tr}(Y_d^a Y_d^{b\dagger}) + \text{Tr}(Y_e^a Y_e^{b\dagger}). \quad (18)$$

The index of the Higgs bosons $b = 1, 2$ is summed over. The RGEs of the gauge coupling constants are given by ⁸

$$16\pi^2 \mu \frac{d}{d\mu} g_i = b_i g_i^3, \quad (b_1, b_2, b_3) = (-3, 6, 18), \quad (19)$$

where $(g_1, g_2, g_3) = (g', g, g_s)$ are the gauge coupling constants of $U(1)_Y$, $SU(2)_L$ and $SU(3)_C$, respectively. The beta function of the gauge coupling constants includes the contributions from the triplets, Δ_L and $\bar{\Delta}_L$.

⁷In this paper, we do not consider RGE contributions from λ_{ij}^ν in Eq. (11). This is justified if the Yukawa coupling λ^ν is negligible and/or Δ_L is heavier than μ_R . The study for the sizable λ^ν with light Δ_L is interesting, but beyond the scope of this paper.

⁸The index $i = 1, 2, 3$ is not summed on the right-hand side.

3.2 The SM fermion masses

At the SUSY breaking scale, $\mu_S \sim \mathcal{O}(100)$ TeV, the SUSY particles and three of the four Higgs doublets are integrated out. In the basis of the Higgs doublets, $\hat{H} = (\hat{H}_1, \hat{H}_2, \hat{H}_3, \hat{H}_4) = (\tilde{H}_u^1, \tilde{H}_u^2, H_d^1, H_d^2)$ with $\tilde{H}_u^a := \tau_2 H_u^{a*}$, the Higgs mass matrix, defined as $V_H \supset \hat{H}^\dagger M_H^2 \hat{H}$, is given by

$$M_H^2 = \begin{pmatrix} |\mu_1|^2 + (m_{H_u}^2)_{11} & (m_{H_u}^2)_{21} & B_{11} & B_{21} \\ (m_{H_u}^2)_{12} & |\mu_2|^2 + (m_{H_u}^2)_{22} & B_{12} & B_{22} \\ B_{11}^* & B_{12}^* & |\mu_1|^2 + (m_{H_d}^2)_{11} & (m_{H_d}^2)_{12} \\ B_{21}^* & B_{22}^* & (m_{H_d}^2)_{21} & |\mu_2|^2 + (m_{H_d}^2)_{22} \end{pmatrix}, \quad (20)$$

where the contributions from the Higgs VEVs are neglected. The mass basis of the Higgs bosons are defined as

$$\hat{H}_I = \sum_{J=1}^4 U_{IJ} H_J, \quad U^\dagger M_H^2 U = \text{diag}(0, m_{H_2}, m_{H_3}, m_{H_4}), \quad (21)$$

where U is a unitary matrix. Here, $I = 1, 2, 3, 4$. In the decoupling limit, we expect that the VEVs of the doublets are aligned as the direction of the massless mode, i.e. $\langle H_I \rangle = v_H \delta_{I1}$, where $v_H \simeq 174$ GeV. Note that the lightest mode is massless up to $\mathcal{O}(v_H^2)$ after imposing the vacuum condition⁹ and is corresponding to the SM-like Higgs doublet, $h_{\text{SM}} := H_1$. The Yukawa couplings in the mass basis of the Higgs bosons are given by

$$-\mathcal{L}_{\text{yuk}}^H = (Y_u^{H_I})_{ij} \tilde{H}_I \tau_2 \hat{Q}_L^i \hat{u}_R^{c,j} + (Y_d^{H_I})_{ij} H_I \tau_2 \hat{Q}_L^i \hat{d}_R^{c,j} + (Y_e^{H_I})_{ij} H_I \tau_2 \hat{L}_L^i \hat{e}_R^{c,j} + h.c., \quad (22)$$

where the Yukawa matrices are

$$Y_u^{H_I} = \sum_{a=1,2} U_{aI}^* Y_u^a(\mu_S), \quad Y_d^{H_I} = \sum_{a=1,2} U_{2+a,I} Y_d^a(\mu_S), \quad Y_e^{H_I} = \sum_{a=1,2} U_{2+a,I} Y_e^a(\mu_S). \quad (23)$$

Here the flavor indices of the quarks and leptons are omitted. The SM fermion mass matrices at $\mu = \mu_S$ are thus given by

$$M_u = Y_u^{h_{\text{SM}}} v_H, \quad M_d = Y_d^{h_{\text{SM}}} v_H, \quad M_e = Y_e^{h_{\text{SM}}} v_H. \quad (24)$$

Defining the diagonalization unitary matrices as

$$U_{fL}^\dagger M_f U_{fR} = \text{diag}(m_{f_1}, m_{f_2}, m_{f_3}), \quad f = u, d, e, \quad (25)$$

the CKM matrix is given by $V_{\text{CKM}} = U_{uL}^\dagger U_{dL}$. These should be consistent with the observed fermion masses and the CKM matrix. In the analysis of the next section, we will study the flavor violations via the Yukawa couplings with the heavy Higgs bosons

⁹See, e.g. Appendix A of Ref. [78] for more explicit formulas.

which are unavoidably correlated with the SM Yukawa couplings through the matching conditions Eqs. (14) and (23).

After the LR symmetry breaking and integrating out the right-handed neutrinos, the effective superpotential is derived as

$$W_{\text{eff}}^N = -\frac{1}{2} \left(\hat{L}_L^i \tau_2 H_u^a \right) Y_{ij}^{\ell a} (M_R^{-1})_{jk} Y_{mk}^{\ell b} \left(\hat{L}_L^m \tau_2 H_u^b \right), \quad (26)$$

where the Majorana mass matrix for the right-handed neutrinos is defined as $(M_R)_{ij} := \lambda_{ij}^\nu v_R$. After the EW symmetry breaking, the neutrino mass matrix is given by

$$\hat{m}_\nu = \frac{v_H^2}{2} Y_\nu^{h_{\text{SM}}} M_R^{-1} Y_\nu^{h_{\text{SM}T}}, \quad Y_\nu^{h_{\text{SM}}} = U_{a1}^* Y^{\ell a}. \quad (27)$$

This can be diagonalized by a unitary matrix U_n , i.e.

$$U_n^T \hat{m}_\nu U_n = \text{diag}(m_{\nu_1}, m_{\nu_2}, m_{\nu_3}). \quad (28)$$

The diagonal values m_{ν_i} and the Pontecorvo-Maki-Nakagawa-Sakata (PMNS) matrix, $U_{\text{PMNS}} := U_{eL}^\dagger U_n$, should be consistent with the observed mass squared differences and mixing angles, respectively.

3.3 Parametrization and outline of numerical analysis

We study how flavor physics depends on the mass matrices of the quarks, leptons and Higgs bosons in this model. There are four hermitian Yukawa matrices, Y^a and $Y^{\ell a}$, a Yukawa matrix for the Majorana masses, λ^ν , μ parameters μ^{ab} and soft SUSY breaking parameters. We assume that the SUSY particles are so heavy that these are irrelevant to the flavor observables in the analysis. The neutrino masses and mixings depend on $Y^{\ell a}$, λ^ν and μ_R . In the numerical analysis, the RG contribution from λ^ν is ignored, assuming it is negligibly small and/or Δ_L is decoupled at a sufficiently high scale.

We parametrize the direction of the SM Higgs boson, h_{SM} , in the four Higgs bosons as

$$h_{\text{SM}} = s_\beta s_{\theta_u} \hat{H}_1 + s_\beta c_{\theta_u} \hat{H}_2 + c_\beta s_{\theta_d} \hat{H}_3 + c_\beta c_{\theta_d} \hat{H}_4, \quad (29)$$

where $s_\theta = \sin \theta$ and $c_\theta = \cos \theta$ with $\theta = \theta_u, \theta_d$ and β . Here β is defined by analogy with the 2HDM, so that $\tan \beta := \sin \beta / \cos \beta$ is a ratio of VEVs of the up-type to down-type Higgs bosons. We assume that the Higgs mass matrix is real and the eigenvalues for the three heavy states have a common mass m_H^2 . We parametrize the orthogonal matrix U as

$$U = U^0 U^3, \quad U^0 := \begin{pmatrix} s_\beta s_{\theta_u} & c_{\theta_u} & 0 & c_\beta s_{\theta_u} \\ s_\beta c_{\theta_u} & -s_{\theta_u} & 0 & c_\beta c_{\theta_u} \\ c_\beta s_{\theta_d} & 0 & c_{\theta_d} & -s_\beta s_{\theta_d} \\ c_\beta c_{\theta_d} & 0 & -s_{\theta_d} & -s_\beta c_{\theta_d} \end{pmatrix}, \quad U^3 := \begin{pmatrix} 1 & 0_{1 \times 3} \\ 0_{3 \times 1} & u_3 \end{pmatrix}, \quad (30)$$

where u_3 is a 3×3 orthogonal matrix. As will be shown in Sec. 4.1, u_3 is irrelevant to four fermi interactions induced by the heavy Higgs bosons under the assumption of the common mass for the heavy Higgs bosons. With this parametrization, the SM Higgs Yukawa couplings in Eq. (23) are given by

$$Y_u^{h_{\text{SM}}} = s_\beta s_{\theta_u} Y_u^1 + s_\beta c_{\theta_u} Y_u^2, \quad Y_d^{h_{\text{SM}}} = c_\beta s_{\theta_d} Y_d^1 + c_\beta c_{\theta_d} Y_d^2, \quad Y_e^{h_{\text{SM}}} = c_\beta s_{\theta_d} Y_e^1 + c_\beta c_{\theta_d} Y_e^2. \quad (31)$$

Note that these relations are satisfied at the SUSY breaking scale $\mu = \mu_S$. We require that these are matched with the Yukawa matrices extrapolated via the RGEs [79] from the boundary conditions at the EW scale μ_{EW} ,

$$Y_u^{h_{\text{SM}}}(\mu_{\text{EW}}) = v_H^{-1} \text{diag}(m_u, m_c, m_t), \quad Y_d^{h_{\text{SM}}}(\mu_{\text{EW}}) = v_H^{-1} V_{\text{CKM}}^\dagger \text{diag}(m_d, m_s, m_b), \\ Y_e^{h_{\text{SM}}}(\mu_{\text{EW}}) = v_H^{-1} \text{diag}(m_e, m_\mu, m_\tau). \quad (32)$$

For concreteness, we choose the Higgs mixing angles as

$$\tan \beta = 3, \quad \sin \theta_u = \cos \theta_d = 0.9999. \quad (33)$$

$\tan \beta$ is chosen such that the 125 GeV Higgs boson mass is explained in the high-scale SUSY breaking scenario [80, 81]. It is notable that from these papers, $2 \lesssim \tan \beta \lesssim 7$ is necessary to reproduce Higgs mass for high scale SUSY. We will later comment on effects to flavor predictions when the value of $\tan \beta$ is changed. $\cos \theta_d = 0.9999$ is fixed so that the realistic Yukawa and CKM parameters are realized by our numerical fitting. See, the relevant discussion in Sec. 4.2 and Appendix A for more details. Note that the parameter setting in Eq. (33) is one benchmark for the analysis, and we checked that our fit procedure can be used for other parameter cases. This hierarchy in VEV is introduced such that the up-type Yukawa couplings are dominantly given by $Y_u^1 \sim Y^1$, while the down-type Yukawa couplings are dominantly given by $Y_d^2 \sim Y^2$ ¹⁰. Such hierarchical VEVs will be realized by a hierarchy in the SUSY breaking parameters [78]. In the numerical analysis, the four hermitian matrices, Y^a and $Y^{\ell a}$, at the LR symmetry breaking scale are tuned to realize these Yukawa matrices consistent with the quark/lepton masses and the CKM matrix at $\mu = \mu_S$.

In our analysis, we parametrize Y_e^a as

$$Y_e^1(\mu_R) = U_\ell^\dagger D_3 U_\ell, \quad Y_e^2(\mu_R) = D_4, \quad (34)$$

where U_ℓ is the unitary matrix, and $D_{3,4}$ are 3×3 real diagonal matrices. The neutrino mass differences and the PMNS matrix are realized by tuning the Majorana mass matrices corresponding to given $Y_e^{1,2}$. Note that D_4 is used to realize the charged lepton masses. U_ℓ and D_3 are treated as free parameters for the fitting procedure.

¹⁰In fact, we could not find a good parameter set for the realistic Yukawa couplings if we do not assume this hierarchy. Actually, $\sin \theta_u \sim 1$ and $\cos \theta_d \sim 1$ are necessary for fitting the CKM matrix. In our analysis, $\sin \theta_u$ is set to be same value as $\cos \theta_d$ for reducing model parameters. Even if $\sin \theta_u \neq \cos \theta_d$, predictions of flavor processes will not be drastically changed.

4 Flavor physics induced by heavy Higgs

In this section, we shall discuss flavor physics in the model. The flavor violations via the heavy Higgs bosons exchanging are unavoidable in the LR symmetric model due to the mixing of the Yukawa matrices even if hierarchical VEV alignment of the Higgs bosons is assumed. The flavor violating Yukawa couplings of heavy Higgs induce FCNCs at the tree level. We shall study testability of those effects in the current and future experiments. In our analysis, the heavy Higgs mass m_H is assumed to be $\mathcal{O}(100)$ TeV. We note that the heavy Higgs bosons could be much lighter than the other SUSY particles, e.g. in the mirage mediation as studied in Ref. [76].

For convenience, we define the Dirac fermions,

$$\psi_f = \begin{pmatrix} f_R^c \\ f_L^\dagger \end{pmatrix}, \quad \bar{\psi}_f = (f_L \ f_R^{c\dagger}), \quad f = u, d, e. \quad (35)$$

The four fermi interactions, after integrating out the heavy neutral Higgs bosons, are given by

$$\begin{aligned} \mathcal{L}_{4F} = \frac{1}{m_H^2} \sum_{A=2,3,4} & \left(\bar{\psi}_u \tilde{Y}_u^{HA} P_L \psi_u - \bar{\psi}_d \tilde{Y}_d^{HA \dagger} P_R \psi_d - \bar{\psi}_e \tilde{Y}_e^{HA \dagger} P_R \psi_e \right) \\ & \times \left(\bar{\psi}_u \tilde{Y}_u^{HA \dagger} P_R \psi_u - \bar{\psi}_d \tilde{Y}_d^{HA} P_L \psi_d - \bar{\psi}_e \tilde{Y}_e^{HA} P_L \psi_e \right), \end{aligned} \quad (36)$$

where, the chirality projection operators are defined as

$$P_L = \begin{pmatrix} 1 & 0 \\ 0 & 0 \end{pmatrix}, \quad P_R = \begin{pmatrix} 0 & 0 \\ 0 & 1 \end{pmatrix}. \quad (37)$$

The Yukawa matrices \tilde{Y}_f^{HA} are the Yukawa matrices in the mass basis,

$$\tilde{Y}_f^{HA} := U_{fL}^\dagger Y_f^{HA} U_{fR}, \quad f = u, d, e, \quad (38)$$

where the Yukawa matrices in the gauge basis of the fermions are given in Eq. (23). For later, we also define the Yukawa matrices in the fermion mass basis and the Higgs basis before the mass diagonalization as

$$\tilde{Y}_f^a = U_{fL}^\dagger Y_f^a U_{fR}, \quad a = 1, 2. \quad (39)$$

4.1 $\Delta F = 2$ processes

The neutral meson mixing is the most sensitive to the FCNCs in the quark sector induced by neutral boson exchanging. The relevant term for $\Delta F = 2$ processes is given by

$$\mathcal{H}_{\text{eff}}^{\Delta F=2} = -(C_4^d)_{ij} \left(\bar{\psi}_d^i P_R \psi_d^j \right) \left(\bar{\psi}_d^i P_L \psi_d^j \right) + h.c., \quad (40)$$

where the Wilson coefficient is ¹¹

$$\begin{aligned}
(C_4^d)_{ij} &= \frac{1}{m_H^2} \sum_{A=2,3,4} \left(\tilde{Y}_d^{HA} \right)_{ji}^* \left(\tilde{Y}_d^{HA} \right)_{ij} \\
&= \frac{1}{m_H^2} \sum_{A=2,3,4} \left(\sum_{a=1,2} U_{2+a,A}^0 \tilde{Y}_d^a \right)_{ji}^* \left(\sum_{b=1,2} U_{2+b,A}^0 \tilde{Y}_d^b \right)_{ij}.
\end{aligned} \tag{41}$$

The second equality is derived from Eqs. (23) and (30). Note that this is independent of U^3 in Eq. (30) after summing over the heavy Higgs bosons with a universal masses ¹². This feature also arises in the other combinations of the four fermi operators.

Before discussing the model predictions of the $\Delta F = 2$ processes, we show the explicit values of Yukawa couplings $\tilde{Y}_d^{1,2}$ at $\mu = \mu_S$ below:

$$\begin{aligned}
\tilde{Y}_d^1 &= \begin{pmatrix} 1.903 \times 10^{-4} & (8.204 \times 10^{-4}) \cdot e^{-3.010i} & (6.662 \times 10^{-3}) \cdot e^{0.3842i} \\ (8.204 \times 10^{-4}) \cdot e^{3.010i} & 3.758 \times 10^{-3} & (3.108 \times 10^{-2}) \cdot e^{3.123i} \\ (6.620 \times 10^{-3}) \cdot e^{-0.3842i} & (3.106 \times 10^{-2}) \cdot e^{-3.123i} & 0.7453 \end{pmatrix}, \\
\tilde{Y}_d^2 &= \begin{pmatrix} 3.190 \times 10^{-5} & (1.160 \times 10^{-5}) \cdot e^{0.1321i} & (9.372 \times 10^{-5}) \cdot e^{-2.757i} \\ (1.160 \times 10^{-5}) \cdot e^{-0.1321i} & 6.365 \times 10^{-4} & (4.396 \times 10^{-4}) \cdot e^{-0.01814i} \\ (9.363 \times 10^{-5}) \cdot e^{2.757i} & (4.393 \times 10^{-4}) \cdot e^{0.01814i} & 2.414 \times 10^{-2} \end{pmatrix}.
\end{aligned} \tag{42}$$

Throughout the paper, we set $\mu_S = 100$ TeV as a reference scale for the analysis. These matrices can realize the SM Higgs Yukawa couplings correctly with the Higgs mixing angles in Eq. (33).

Here, we show the values with $U_\ell = 1_{3 \times 3}$. The phases of quarks are chosen such that the CKM phases agree with the Wolfenstein parametrization. We numerically checked that the values of the quark Yukawa couplings shown in Eqs. (42) and (43) are almost independent of our choice of U_ℓ . This means that the RG effects through e.g. $Y_d^b \text{Tr}(Y_e^a Y_e^{b\dagger})$ term in Eq. (16), are negligible with our choice of D_3 parameters. We also see that the hermitian structure of the Yukawa matrices are approximately hold in Eqs. (42) and (43) due to the small Yukawa coupling to the light flavors, and thus the LR breaking effect through the RG effects are not significant. Note that there is a possibility to enhance the LR breaking effect by considering λ_{ij}^ν contributions in Eq. (11). However, the analysis will be complicated in this case, and we postpone this issue as a future work.

For predictions of meson mixings, we adopt the notation of the UTfit collaboration [82,

¹¹We calculate the Wilson coefficients of the four fermi operators with the Yukawa couplings directly obtained by solving the RGEs. This is unlike the previous work in which the RG effects are absorbed by the cutoff scale parameter $\Lambda_{qq'}$. In this simplification, however, the effects of $Y_u^a \neq Y_d^a$ originated from the RGE effects were neglected.

¹²The breaking of the mass degeneracy is $\mathcal{O}(v_H)$, and negligible when $v_H \ll m_H$ is satisfied.

83] to see the deviations from the SM predictions. For K - \bar{K} mixing,

$$C_{\Delta M_K} = \frac{\text{Re}[\langle K | \mathcal{H}_{\text{eff}}^{\text{SM+NP}} | \bar{K} \rangle]}{\text{Re}[\langle K | \mathcal{H}_{\text{eff}}^{\text{SM}} | \bar{K} \rangle]}, \quad C_{\epsilon_K} = \frac{\text{Im}[\langle K | \mathcal{H}_{\text{eff}}^{\text{SM+NP}} | \bar{K} \rangle]}{\text{Im}[\langle K | \mathcal{H}_{\text{eff}}^{\text{SM}} | \bar{K} \rangle]}, \quad (44)$$

and for B_q - \bar{B}_q mixing,

$$C_{B_q} e^{2i\phi_{B_q}} = \frac{\langle B_q | \mathcal{H}_{\text{eff}}^{\text{SM+NP}} | \bar{B}_q \rangle}{\langle B_q | \mathcal{H}_{\text{eff}}^{\text{SM}} | \bar{B}_q \rangle}. \quad (45)$$

Then, $C_{\Delta M_K} = 1$, $C_{\epsilon_K} = 1$, $C_{B_q} = 1$ and $\phi_{B_q} = 0$, when the new physics (NP) contribution is vanishing. The UTfit collaboration has presented the global fit for the NP contributions, and the results are ¹³

$$C_{\epsilon_K} = 1.12 \pm 0.12, \quad (46)$$

$$C_{B_d} = 1.05 \pm 0.11, \quad \phi_{B_d} [\text{rad}] = -0.035 \pm 0.031, \quad (47)$$

$$C_{B_s} = 1.110 \pm 0.090, \quad \phi_{B_s} [\text{rad}] = 0.0073 \pm 0.0155. \quad (48)$$

In Ref. [83], we can find $C_{\Delta M_K} = 0.93 \pm 0.32$ which is consistent with the SM prediction within the uncertainty. The matrix element $\langle M | \mathcal{H}_{\text{eff}} | \bar{M} \rangle$ relevant to the oscillation matrix element M_{12}^M can be divided into SM and NP contributions, $M_{12}^M = (M_{12}^M)_{\text{SM}} + (M_{12}^M)_{\text{NP}}$. Each SM contribution can be found in Ref. [84], and the contributions including the QCD running effects can be estimated by

$$(M_{12}^M)_{\text{NP}}^* = -\frac{1}{2m_M} (C_4^d)_{ij} \langle M | Q_{ij}^{LR} | \bar{M} \rangle, \quad (49)$$

where $M = K, B_d, B_s$, $Q_{ij}^{LR} = (\bar{d}_L^i d_R^j)(\bar{d}_R^i d_L^j)$, and we only show the leading part for the model. The explicit descriptions are discussed in Refs. [85, 86]. Since the QCD running correction is sizable, we take the explicit values, shown in Table 9 in Ref. [87], for the operators, $\mathcal{O}_M^{LR} \equiv \langle M | Q_{ij}^{LR} | \bar{M} \rangle / (2m_M)$:

$$\mathcal{O}_K^{LR} = 0.261, \quad \mathcal{O}_{B_d}^{LR} = 0.241, \quad \mathcal{O}_{B_s}^{LR} = 0.338. \quad (50)$$

The other parameters used in the analysis are summarized in Table 2. We show the prediction of C_{ϵ_K} in Fig. 1 with red band. To draw the prediction, we used the central values for the input parameters summarized in Table 2. The width of the red band stems from different structures of U_ℓ and our fit prescription. See, Appendix A for detail. The horizontal axis is heavy Higgs mass m_H in unit of TeV. The dark and light blue bands show the UTfit result [82, 83] within 1σ and 2σ , respectively. Since the model predicts $C_{\epsilon_K} < 1$ while the UTfit result favors $C_{\epsilon_K} > 1$, the prediction cannot be within the 1σ error of the UTfit result even when $m_H > \mathcal{O}(100)$ TeV. If we accept 2σ deviation, the

¹³The latest results can be found at <http://www.utfit.org/UTfit/WebHome>.

$m_d(2 \text{ GeV})$	$4.67_{-0.17}^{+0.48} \text{ MeV}$ [88]	$m_s(2 \text{ GeV})$	$93_{-5}^{+11} \text{ MeV}$ [88]
m_K	$497.611(13) \text{ MeV}$ [88]	η_1	1.87 ± 0.76 [89]
η_2	0.5765 ± 0.0065 [90]	η_3	0.496 ± 0.047 [91]
F_K	$156.3(0.9) \text{ MeV}$ [92]	\hat{B}_K	$0.7625(97)$ [93]
$m_b(m_b)$	$4.18_{-0.02}^{+0.03} \text{ GeV}$ [88]	η_B	0.55 ± 0.01 [90, 94]
m_{B_d}	$5.27965(12) \text{ GeV}$ [88]	m_{B_s}	$5.36688(14) \text{ GeV}$ [88]
$F_{B_d} \sqrt{\hat{B}_{B_d}}$	$225(9) \text{ MeV}$ [93]	$F_{B_s} \sqrt{\hat{B}_{B_s}}$	$274(8) \text{ MeV}$ [93]

Table 2: The input parameters relevant to the analyses on flavor physics. We use the central value of those parameters in the numerical analysis.

lower bound on m_H is given by $m_H > 165 \text{ TeV}$. We checked that the lower bound on m_H from C_{ϵ_K} is the most stringent in the flavor observables which we studied. The deviations from the SM predictions are smaller than 1% in $C_{\Delta M_K}$ and C_{B_q} , when $m_H = \mathcal{O}(100) \text{ TeV}$. The deviation of ϕ_{B_q} is extremely small: $\phi_{B_q} \approx 0$. Therefore, we conclude that the UTfit results within 2σ can be achieved by setting $m_H > 165 \text{ TeV}$. Note that even when we change the benchmark value in Eq. (33), the lower bound on m_H will be around $160 \sim 170 \text{ TeV}$. Hereafter, we set $m_H = 170 \text{ TeV}$ as a reference value for the remaining discussions, although some points do not satisfy the 2σ result of the UTfit result for C_{ϵ_K} . For general m_H , all the branching ratios studied in the next section can be obtained by multiplying $(170 \text{ TeV}/m_H)^4$.

Note that as long as we consider the lower bound on m_H from ϵ_K constraint, the other FCNC processes are suppressed. For example, our contributions to ϵ'/ϵ ,¹⁴ which is one of important $\Delta F = 1$ processes are negligible since relevant Wilson coefficients are quite small, $\mathcal{O}(10^{-8})/m_H^2$ from Eqs. (42) and (43).

4.2 LFV processes

In this section, we show the model predictions of the LFV processes, especially $e_i^- \rightarrow e_k^+ e_j^- e_l^-$ and the μ - e conversion process. Since there are degrees of freedom originated from the arbitrary unitary matrix U_ℓ and real diagonal matrix D_3 in Eq. (34), the predictions strongly depend on these parameters in lepton sector. Actually, these structures change the numerical results of $\tilde{Y}_e^{H_I}$ at $\mu_S = 100 \text{ TeV}$; e.g., $\tilde{Y}_e^{H_3} = c_{\theta_d} \tilde{Y}_e^1(\mu_S) - s_{\theta_d} \tilde{Y}_e^2(\mu_S) \sim \tilde{Y}_e^1(\mu_S)$. In particular, the size of D_3 directly relates to not only the size of LFV predictions but also the Majorana scale μ_{ν_R} . See Appendix A for the detail about how to fix D_3 for the analysis. We scan over the parameters in U_ℓ with fixed values in D_3 , and generated about 7000 samples which reproduce fermion masses and CKM parameters.

For charged lepton decays $e_i^- \rightarrow e_k^+ e_j^- e_l^-$, the branching ratios are calculated with the

¹⁴The discussion of the sizes of each Wilson coefficient for this observable, see Ref. [95].

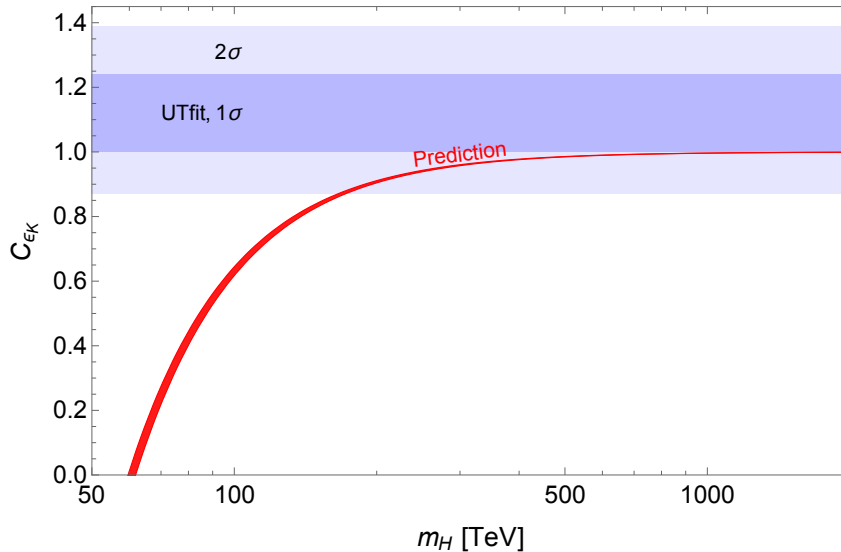


Figure 1: The model prediction for C_{ϵ_K} as a function of heavy Higgs mass m_H is shown by red band. The horizontal blue bands show the UTfit result within 1σ (darker) and 2σ (lighter) [82, 83].

four fermi operator, $(C_4^e)^{kl}(\bar{e}_L^i e_R^j)(\bar{e}_R^k e_L^l)$. The Wilson coefficient is defined as

$$(C_4^e)^{kl} = \frac{1}{m_H^2} \sum_{A=2,3,4} \left(\tilde{Y}_e^{H_A} \right)_{ji}^* \left(\tilde{Y}_e^{H_A} \right)_{kl}, \quad (51)$$

and this can be calculated in the same manner as in Eq. (41). The branching ratios can be estimated in the limit that the daughter leptons are massless [39]. For $e_i^- \rightarrow e_j^+ e_k^- e_k^-$ decays (both for $j = k$ and $j \neq k$),

$$\text{BR}(e_i^- \rightarrow e_j^+ e_k^- e_k^-) = \frac{m_{e_i}^5 \tau_{e_i}}{6144\pi^3} \left(|(C_4^e)^{kj}|^2 + |(C_4^e)^{ki}|^2 \right), \quad (52)$$

and for $e_i^- \rightarrow e_j^+ e_j^- e_k^-$ decays with $j \neq k$,

$$\text{BR}(e_i^- \rightarrow e_j^+ e_j^- e_k^-) = \frac{m_{e_i}^5 \tau_{e_i}}{6144\pi^3} \left(|(C_4^e)^{jj}|^2 + |(C_4^e)^{ki}|^2 + |(C_4^e)^{kj}|^2 + |(C_4^e)^{ji}|^2 \right). \quad (53)$$

In particular, we show the correlation among these branching ratios. The predictions of $\text{BR}(\mu \rightarrow 3e)$ and $\text{BR}(\tau \rightarrow 3e)$ are shown in Fig. 2. In this plot, we set $m_H = 170$ TeV, and in this case, some points do not satisfy 2σ result of the UTfit for C_{ϵ_K} , which are shown in blue. The green dashed line is the future prospect of $\text{BR}(\mu \rightarrow 3e)$ [96]. For the muon decay, the maximal values are $\text{BR}(\mu \rightarrow 3e) \simeq 3.4 \times 10^{-15}$. Although this is about 0.003 times smaller than the current upper bound, $\text{BR}(\mu \rightarrow 3e) < 10^{-12}$ [97], it exceeds the future prospect of Mu3e experiment, $\text{BR}(\mu \rightarrow 3e) < 10^{-16}$ [96]. Therefore, there is a possibility to detect our signal in the future experiment. Note that the predictions

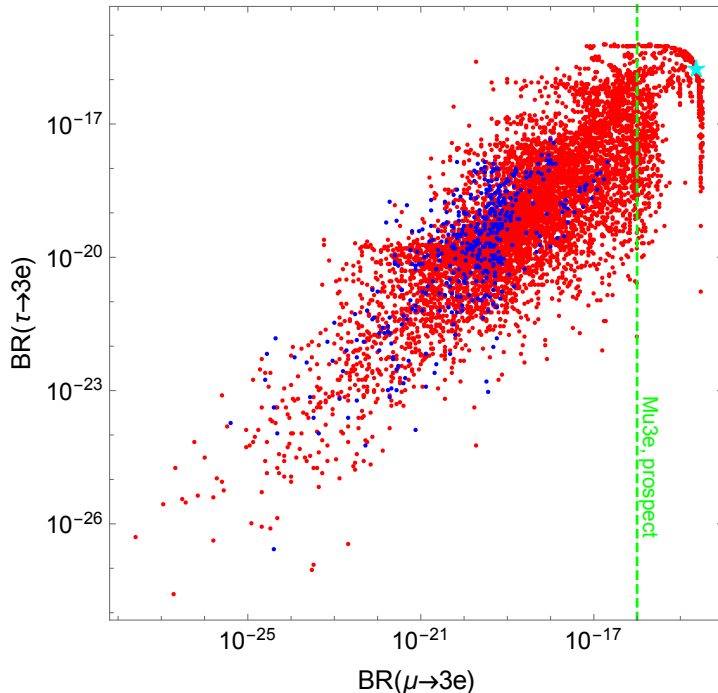


Figure 2: Correlation between our predictions of $\text{BR}(\mu \rightarrow 3e)$ and $\text{BR}(\tau \rightarrow 3e)$. We set $m_H = 170$ TeV for the plot. The red points satisfy the UTfit result of C_{e_K} within 2σ , while the blue ones do not satisfy it. The green dashed line corresponds to the future prospect [96]. The right-upper cyan star is the benchmark point for Eq. (54).

are enhanced by choosing larger $\tan\beta$ than Eq. (33). For example, when $\tan\beta = 6$, the prediction of $\mu \rightarrow 3e$ is enhanced by one order of magnitude. In that case, we can investigate more broader parameter space by future experiments.

For τ decay processes, the maximal prediction for $\text{BR}(\tau \rightarrow 3e)$ is 6.0×10^{-16} . Compared with the current upper bound $\text{BR}(\tau \rightarrow 3e) < 2.7 \times 10^{-8}$ [88], it is difficult to reach the bound when $m_H = \mathcal{O}(100)$ TeV. The branching ratios for the other τ decay processes are also small, $\text{BR}(\tau^- \rightarrow e_i^+ e_j^- e_k^-) \lesssim \mathcal{O}(10^{-15})$.

The cyan star in Fig. 2 shows the prediction when the sum of the Yukawa matrices is given by

$$\left| \sum_{A=2,3,4} \tilde{Y}_e^{HA} \right| = \begin{pmatrix} 0.320 & 0.199 & 0.130 \\ 0.204 & 0.144 & 0.0666 \\ 0.134 & 0.0676 & 0.0370 \end{pmatrix} \quad (54)$$

which leads to the Wilson coefficient for $\mu \rightarrow 3e$ as $(C_4^e)_{11}^{12} \simeq 2.2 \times 10^{-12}$ with $m_H = 170$ TeV.

The low density around $\text{BR}(\mu \rightarrow 3e) \sim \mathcal{O}(10^{-15})$ and $\text{BR}(\tau \rightarrow 3e) \leq 10^{-17}$ in Fig. 2 is due to the failure of the fit to realize the electron mass. In our fit procedure, we start the iteration with the estimated values obtained from the experimental values via the

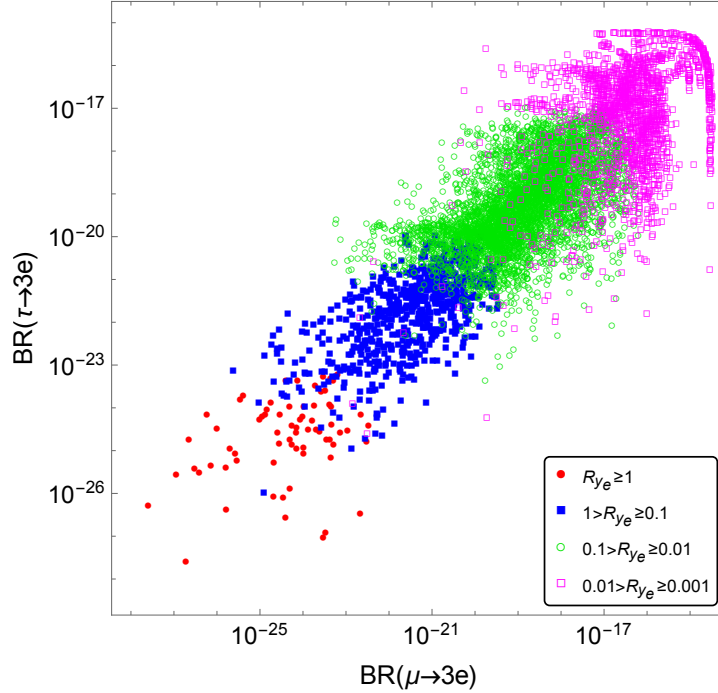


Figure 3: Same plot as Fig. 2. The red filled circle, blue filled square, green circle and magenta square correspond to $R_{y_e} \geq 1$, $1 > R_{y_e} \geq 0.1$, $0.1 > R_{y_e} \geq 0.01$ and $0.01 > R_{y_e} \geq 0.001$, respectively.

approximate RGE. Therefore $(Y_e^2)_{11}$ will be the main component of the electron Yukawa coupling y_e and its size is $\mathcal{O}(10^{-6})$. However, if there is a large contribution from Y_e^1 through the RGE, $(Y_e^2)_{11}$ will be larger than 10^{-6} and cancellation between Y_e^1 and Y_e^2 to obtain correct electron Yukawa coupling is required. In this case, the fit procedure may tend to fail due to the tuning for y_e . In order to see this feature, we define the following parameter which is corresponding to the tuning level of y_e :

$$R_{y_e} := \left(c_\beta s_{\theta_d} (\tilde{Y}_e^1)_{11} + c_\beta c_{\theta_d} (\tilde{Y}_e^2)_{11} \right) / \text{Max} \left(c_\beta s_{\theta_d} (\tilde{Y}_e^1)_{11}, c_\beta c_{\theta_d} (\tilde{Y}_e^2)_{11} \right). \quad (55)$$

$R_{y_e} \ll 1$ means that a severe tuning is required by y_e . Fig. 3 shows the same plot as Fig. 2 using the same data and different color manner depending on the values of R_{y_e} . The red filled circle, blue filled square, green circle and magenta square correspond to $R_{y_e} \geq 1$, $1 > R_{y_e} \geq 0.1$, $0.1 > R_{y_e} \geq 0.01$ and $0.01 > R_{y_e} \geq 0.001$, respectively. In this plot, we omit the future prospect for $\text{BR}(\mu \rightarrow 3e)$ for simplicity. The low density area mentioned above can be read as the case of $0.01 > R_{y_e} \geq 0.001$. Therefore, the main reason for the low density of the scattering plots is due to the failure of the fit to y_e . We also see that the larger LFV effects are induced when there is the severer tuning for y_e . This relation between the tuning level and LFV prediction is one of the important observations of our new analysis.

Next, we discuss the predictions for the μ - e conversion in nuclei. The relevant four fermi operators are

$$\begin{aligned} \mathcal{L}_{eff}^{\mu-e} = & \sum_{q=d,s} [(C_4^{de})_{qq}^{e\mu} (\bar{q}_L q_R) (\bar{e}_R \mu_L) + (C_4^{de})_{qq}^{\mu e*} (\bar{q}_R q_L) (\bar{e}_L \mu_R)] \\ & + (C_4^{ue})_{uu}^{e\mu} (\bar{u}_R u_L) (\bar{e}_R \mu_L) + (C_4^{ue})_{uu}^{\mu e*} (\bar{u}_L u_R) (\bar{e}_L \mu_R). \end{aligned} \quad (56)$$

The branching ratio of the μ - e conversion can be calculated by following Ref. [98]:

$$\text{BR}(\mu N \rightarrow e N) = \frac{\omega_{\text{conv}}}{\omega_{\text{capt}}}, \quad (57)$$

where in the model,

$$\omega_{\text{conv}} = 2G_F^2 \left(|\tilde{g}_{LS}^{(p)} S^{(p)} + \tilde{g}_{LS}^{(n)} S^{(n)}|^2 + |\tilde{g}_{RS}^{(p)} S^{(p)} + \tilde{g}_{RS}^{(n)} S^{(n)}|^2 \right), \quad (58)$$

$$\tilde{g}_{LS,RS}^{(p)} = \sum_{q=u,d,s} G_S^{(q,p)} g_{LS,RS(q)}, \quad \tilde{g}_{LS,RS}^{(n)} = \sum_{q=u,d,s} G_S^{(q,n)} g_{LS,RS(q)}, \quad (59)$$

and $g_{LS,RS(q)}$ can be described as

$$g_{LS(u)} = -\frac{\sqrt{2}}{2G_F} (C_4^{ue})_{uu}^{\mu e*}, \quad g_{RS(u)} = -\frac{\sqrt{2}}{2G_F} (C_4^{ue})_{uu}^{e\mu}, \quad (60)$$

$$g_{LS(d,s)} = -\frac{\sqrt{2}}{2G_F} (C_4^{de})_{dd,ss}^{\mu e*}, \quad g_{RS(d,s)} = -\frac{\sqrt{2}}{2G_F} (C_4^{de})_{dd,ss}^{e\mu}. \quad (61)$$

The relevant Wilson coefficients are calculated as

$$(C_4^{ue})_{ij}^{kl} = -\frac{1}{m_H^2} \sum_{A=2,3,4} \left(\tilde{Y}_u^{H_A} \right)_{ij} \left(\tilde{Y}_e^{H_A} \right)_{kl}, \quad (62)$$

$$(C_4^{de})_{ij}^{kl} = \frac{1}{m_H^2} \sum_{A=2,3,4} \left(\tilde{Y}_d^{H_A} \right)_{ji}^* \left(\tilde{Y}_e^{H_A} \right)_{kl}. \quad (63)$$

The other parameters used in this paper are listed in Table 3. From these expressions, we find a correlation,

$$\text{BR}(\mu \text{Al} \rightarrow e \text{Al}) \simeq 1.44 \times \text{BR}(\mu \text{Au} \rightarrow e \text{Au}). \quad (64)$$

since they are related to same coefficients, $(C_4^{ue})_{uu}^{e\mu}$, $(C_4^{de})_{dd}^{e\mu}$ and $(C_4^{de})_{ss}^{e\mu}$. Figure 4 shows the scattering plots on $\text{BR}(\mu \rightarrow 3e)$ vs $\text{BR}(\mu \text{Al} \rightarrow e \text{Al})$ plane using the same samples as in Fig. 3. We see that our model predicts $\text{BR}(\mu \text{Al} \rightarrow e \text{Al}) \lesssim 4.3 \times 10^{-13}$ according to current upper bound on $\text{BR}(\mu \text{Au} \rightarrow e \text{Au})$ [100] and Eq. (64), although this bound cannot constrain our model. Some portion of the parameter space will be covered by the future experiments which are sensitive up to $\text{BR}(\mu \text{Al} \rightarrow e \text{Al}) = 3.1 \times 10^{-16}$. The right panel is drawn in the same manner as Fig. 3, and the future prospects shown in the left panel

$G_S^{(u,p)}$	5.1	$\omega_{\text{capt}}(\text{Al})$	4.64×10^{-19}
$G_S^{(d,p)}$	4.3	$S^{(p)}(\text{Al})$	$0.0153m_\mu^{5/2}$
$G_S^{(s,p)}$	2.5	$S^{(n)}(\text{Al})$	$0.0163m_\mu^{5/2}$
$G_S^{(u,n)}$	4.3	$\omega_{\text{capt}}(\text{Au})$	8.60×10^{-18}
$G_S^{(d,n)}$	5.1	$S^{(p)}(\text{Au})$	$0.0523m_\mu^{5/2}$
$G_S^{(s,n)}$	2.5	$S^{(n)}(\text{Au})$	$0.0610m_\mu^{5/2}$

Table 3: The numerical results used for calculation of μ - e conversion [98].

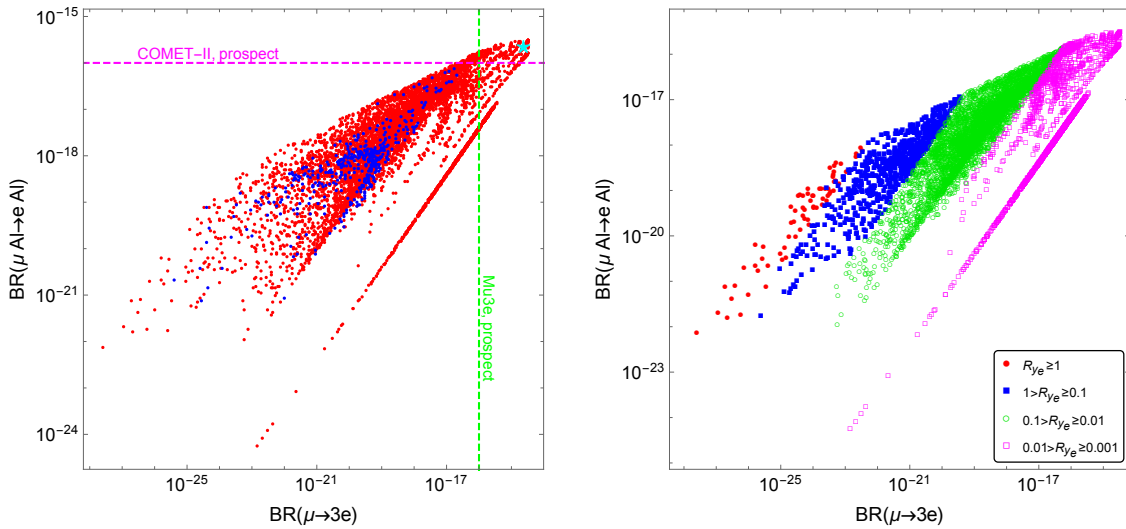


Figure 4: Left: Correlation between our predictions of $\text{BR}(\mu \rightarrow 3e)$ and $\text{BR}(\mu N \rightarrow eN)$ with $m_H = 170$ TeV. The color manner is the same as in Fig. 2, and the magenta dashed line is the expected future sensitivity of $\text{BR}(\mu \text{Al} \rightarrow e \text{Al})$ [99]. Right: The plot for the tuning level in the same plane as the left. We use the same data as in Fig. 2.

are omitted for simplicity. From this figure, the correlation between the size of the LFV prediction and the tuning level of y_e can be seen more clearly. $\text{BR}(\mu \rightarrow 3e)$ is related to $(\tilde{Y}_e^{1,2})_{11}$ and $(\tilde{Y}_e^{1,2})_{12,21}$, and $\text{BR}(\mu \text{Al} \rightarrow e \text{Al})$ is related to $(\tilde{Y}_e^{1,2})_{12,21}$. Note that although $\text{BR}(\mu \text{Al} \rightarrow e \text{Al})$ is also related to Yukawa couplings in the quark sector, these couplings are almost determined in our fit procedure, as mentioned in Sec. 4.1. Once we choose one value of $\text{BR}(\mu \text{Al} \rightarrow e \text{Al})$, which corresponds to set the value of $(\tilde{Y}_e^{1,2})_{12,21}$, the variety of value for $\text{BR}(\mu \rightarrow 3e)$ is dependent on the size of $(\tilde{Y}_e^{1,2})_{11}$. Therefore, the largeness of its size is important to enhance the LFV prediction, while the severe tuning for y_e is needed at the same time.

4.3 Leptonic meson decays

Finally, we discuss leptonic decays of mesons. In the previous two subsections, we have studied the FCNCs in each sector. There we found that m_H should satisfy $m_H > 165$ TeV to evade the ϵ_K bound and the model would be tested by the LFV processes in the future experiments. In the other processes associated with LFV, there will be large deviations from the SM predictions. In the lepton flavor conserving processes, on the other hand, the predictions are the almost same as the SM predictions, because of very large m_H . In this section, we investigate the leptonic meson decays $M \rightarrow \ell\ell'$ ($\ell \neq \ell'$), that are strongly constrained by the experiments. Based on the results of $e_i^- \rightarrow e_j^+ e_k^- e_l^-$, the fit will lead to the large FCNCs that involves first two generations, and thus $K \rightarrow e^\pm \mu^\mp$, $D \rightarrow e^\pm \mu^\mp$ and $B_q \rightarrow e^\pm \mu^\mp$ ($q = d, s$) will be important.

The four fermi operators related to these processes are

$$\mathcal{H}_{eff}^{\Delta F=1} = -(C_4^{de})_{ij}^{kl} (\bar{d}_L^i d_R^j) (\bar{e}_R^k e_L^l) - (C_4^{ue})_{uc}^{kl} (\bar{u}_R c_L) (\bar{e}_R^k e_L^l) + h.c., \quad (65)$$

and the Wilson coefficients are defined in Eqs. (62) and (63). The branching fraction of $K_L \rightarrow e_k \bar{e}_l$, where k, l are the flavor indices, is given by

$$\begin{aligned} \text{BR}(K_L \rightarrow e_k \bar{e}_l) &= \frac{\tau_{K_L}}{128\pi} (m_{e_k} + m_{e_l})^2 m_{K_L} F_K^2 \sqrt{\left(1 - \frac{(m_{e_k} + m_{e_l})^2}{m_{K_L}^2}\right) \left(1 - \frac{(m_{e_k} - m_{e_l})^2}{m_{K_L}^2}\right)} \\ &\times \left\{ \left| \frac{R_{K_L}}{m_{e_k} + m_{e_l}} \{ (C_4^{de})_{sd}^{kl} + (C_4^{de})_{ds}^{lk*} \} - \delta_{kl} C_{\text{SM}}^{sd} \right|^2 \left(1 - \frac{(m_{e_k} - m_{e_l})^2}{m_{K_L}^2}\right) \right. \\ &\left. + \left| \frac{R_{K_L}}{m_{e_k} + m_{e_l}} \{ (C_4^{de})_{sd}^{kl} - (C_4^{de})_{ds}^{lk*} \} \right|^2 \left(1 - \frac{(m_{e_k} + m_{e_l})^2}{m_{K_L}^2}\right) \right\}. \quad (66) \end{aligned}$$

The expressions for $D \rightarrow e^\pm \mu^\mp$ and $B_q \rightarrow e^\pm \mu^\mp$ can be obtained by replacing meson mass, lifetime and decay constant, as well as the Wilson coefficients appropriately. Note that the term $R_{K_L} := m_{K_L}^2 / (m_s + m_d)$ could enhance the scalar contribution massively. C_{SM}^{sd} denotes the SM contribution which is vanishing for the LFV decays. We shall study how these leptonic decays correlate with $\text{BR}(\mu \rightarrow 3e)$ and $\text{BR}(\mu \text{Al} \rightarrow e \text{Al})$.

The prediction for $\text{BR}(K_L \rightarrow e^\pm \mu^\mp)$ is shown in Fig. 5. Again, we set $m_H = 170$ TeV to evade the C_{ϵ_K} bound, and the color manner is same as those in Fig. 4. The predicted values are far below the current bound, $\text{BR}(K_L \rightarrow e^\pm \mu^\mp) < 4.7 \times 10^{-12}$ [101]. As shown in the left panels of Fig. 5 and Fig. 4, the correlation between $\text{BR}(K_L \rightarrow e^\pm \mu^\mp)$ and $\text{BR}(\mu \rightarrow 3e)$ is similar to that between $\text{BR}(\mu \text{Al} \rightarrow e \text{Al})$ and $\text{BR}(\mu \rightarrow 3e)$. This is because both $\text{BR}(K_L \rightarrow e^\pm \mu^\mp)$ and $\text{BR}(\mu \text{Al} \rightarrow e \text{Al})$ depend on $(Y_e^{HA})_{12}$, and therefore, these predictions have the explicit correlation as we can see in the right panel of Fig. 5. We found the following correlation: $\text{BR}(K_L \rightarrow e^\pm \mu^\mp) \simeq 17 \times \text{BR}(\mu \text{Al} \rightarrow e \text{Al})$. Based on this relation,

$$\text{BR}(K_L \rightarrow e^\pm \mu^\mp) \gtrsim 1.7 \times 10^{-15} \quad (67)$$

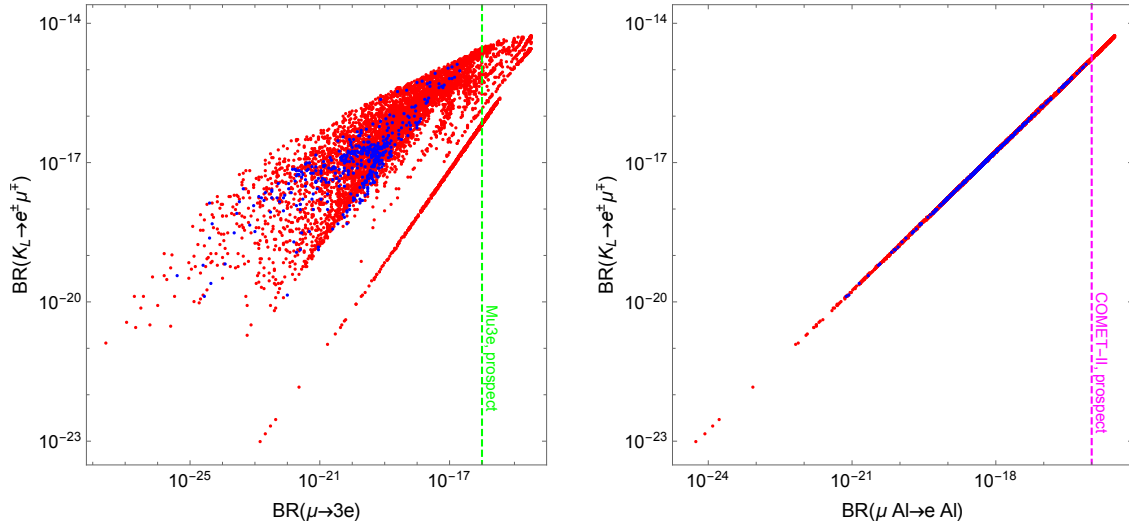


Figure 5: Correlation between $\text{BR}(K_L \rightarrow e^\pm \mu^\mp)$ and LFV predictions with $m_H = 170$ TeV. For this plot, we use the same data as in Fig. 2. The color manner of the points is same as in Fig. 4.

is predicted if the evidence is found in the future experiment for $\mu\text{Al} \rightarrow e\text{Al}$.

The other leptonic meson decays are too small to be probed by the future sensitivities. The maximal values of branching fractions of $D \rightarrow e^\pm \mu^\mp$, $B_d \rightarrow e^\pm \mu^\mp$ and $B_s \rightarrow e^\pm \mu^\mp$ when $m_H = 170$ TeV are respectively about 1.1×10^{-20} , 1.3×10^{-15} and 4.0×10^{-14} , while the upper bounds are respectively 1.3×10^{-8} [102], 1.0×10^{-9} and 5.4×10^{-9} [103]. The other branching ratios for LFV meson decays involving τ in the final state are predicted to be similar values: $\text{BR}(B_d \rightarrow \ell^\pm \tau^\mp) \lesssim 1.1 \times 10^{-15}$ and $\text{BR}(B_s \rightarrow \ell^\pm \tau^\mp) \lesssim 3.5 \times 10^{-14}$ ($\ell = e, \mu$). The current experimental bounds on these processes are $\mathcal{O}(10^{-5})$ [104, 105]. Although their sizes are typically very small, we found the correlation among the branching fractions,

$$\text{BR}(K_L \rightarrow e^\pm \mu^\mp) \simeq (4.8 \times 10^5) \times \text{BR}(D \rightarrow e^\pm \mu^\mp) \quad (68)$$

$$\simeq 4.2 \times \text{BR}(B_d \rightarrow e^\pm \mu^\mp) \quad (69)$$

$$\simeq 0.13 \times \text{BR}(B_s \rightarrow e^\pm \mu^\mp), \quad (70)$$

$$\text{BR}(B_s \rightarrow \ell^\pm \tau^\mp) \simeq 32 \times \text{BR}(B_d \rightarrow \ell^\pm \tau^\mp) \quad (\text{for } \ell = e, \mu). \quad (71)$$

We note that $\text{BR}(K_L \rightarrow e^\pm \mu^\mp)$ also has correlation with $\text{BR}(\mu\text{Al} \rightarrow e\text{Al})$. Since the semi-leptonic decay $K_L \rightarrow \pi e \mu$ gives weaker constraint on corresponding four fermi coefficients than the leptonic decay by two orders of magnitude, as discussed in Ref. [106], the above analysis is enough to discuss the constraint on the model parameters.

5 Summary

In this paper, we have studied the supersymmetric LR model which has four Higgs doublets to reproduce the realistic fermion masses and the CKM matrix. The four Higgs doublets couple to the SM fermions and are mixed with each other, and hence they induce flavor changing couplings at the tree level. We have discussed the predictions of this model with the RGE corrections to Yukawa couplings which were not explicitly taken into account in the previous work [1]. We have numerically studied the corrections, and obtained precise and realistic predictions for flavor processes.

We conclude that ϵ_K is the most important observable and gives the strong constraint on the model. We have investigated the lower bound on m_H and found that $m_H > 165$ TeV is needed to satisfy the UTfit result within 2σ . Note that physical parameters in the quark sector are almost determined by the fermion masses and CKM matrix elements without ambiguity. Due to the large m_H , the other observables related to meson mixings, e.g. C_{B_q} and ϕ_{B_q} , do not largely deviate from the SM predictions.

In contrast, LFV processes like $\mu \rightarrow 3e$ and μ - e conversion can be testable at the future experiments, e.g. Mu3e and COMET-II, as we see in Fig. 4. Note that when such large LFV couplings are obtained, the tuning level of y_e becomes severe because of large RGE corrections from $Y^{\ell 1}$. This relation is an important observation of our improved analysis. We have also discussed the predictions of leptonic meson decays involving LFV couplings, $M \rightarrow \ell\ell'$, and found that the predictions are smaller than the experimental bounds. We observed the correlations among the observables in this model. $\mu \rightarrow 3e$ has the correlation with μ - e conversion as shown in Fig. 4, and there are more clear correlations among μ - e conversion and $M \rightarrow e\mu$, e.g. Fig. 5. Considering these correlations and each experimental bound, we have derived the indirect upper bounds on $M \rightarrow e\mu$, assuming that there is no signal at the future μ - e conversion experiments. The combined search for LFV processes and $M \rightarrow e\mu$ will be another tool to test our model.

In our analysis, we did not consider λ_{ij}^ν contributions to RGE in order to simplify the calculation. However, there is a possibility to observe a significant effect of LR breaking when we consider such contributions properly. In that case, we may be able to obtain different predictions and correlations. We will investigate this possibility in a future work.

Acknowledgments

We thank Nagoya University Theoretical Elementary Particle Physics Laboratory and Motoi Endo for providing computational resources. S. I. would like to thank the warm hospitality at KEK where he stayed during the work. The work of S. I. is supported by the Japan Society for the Promotion of Science (JSPS) Research Fellowships for Young Scientists, No. 19J10980 and the JSPS Core-to-Core Program, No.JPJSCCA20200002. The work of J. K. is supported in by the Institute for Basic Science (IBS-R018-D1), the Department of Energy (DOE) under Award No. DE-SC0011726, and the Grant-in-Aid for

Scientific Research from the Ministry of Education, Science, Sports and Culture (MEXT), Japan No. 18K13534. The work of Y. O. is supported by Grant-in-Aid for Scientific research from MEXT, Japan, No. 19H04614, No. 19H05101, and No. 19K03867. Y. S. thanks for the hospitality of Theoretical Elementary Particle Physics Laboratory, Nagoya University during the work.

A Details of the scan

A.1 Fitting and scanning

We parametrize the four hermitian Yukawa matrices by

$$Y^1 = U_Q^\dagger D_1 U_Q, \quad Y^2 = D_2, \quad Y^{\ell 1} = U_\ell^\dagger D_3 U_\ell, \quad Y^{\ell 2} = D_4, \quad (72)$$

where D_A , $A = 1, 2, 3, 4$, are 3×3 real diagonal matrices. Note that Y^2 and $Y^{\ell 2}$ can be diagonalized without loss of generality.

We fit the three diagonal matrices $D_{1,2,4}$ and the unitary matrix U_Q to be consistent with the fermion masses and CKM matrix at $\mu = \mu_S$, where the values of the Yukawa matrices are given by

$$Y_u^{h\text{SM}}(\mu_S) = \text{diag} (4.97 \times 10^{-6}, 2.51 \times 10^{-3}, 0.717) + \mathcal{O}(10^{-7}) \quad (73)$$

$$Y_d^{h\text{SM}}(\mu_S) = \begin{pmatrix} 1.05 \times 10^{-5} & 4.83 \times 10^{-5} & (4.19 \times 10^{-5}) \cdot e^{-1.24i} \\ (2.42 \times 10^{-6}) \cdot e^{-3.14i} & 2.09 \times 10^{-4} & 4.85 \times 10^{-4} \\ (9.24 \times 10^{-8}) \cdot e^{-0.384i} & (8.48 \times 10^{-6}) \cdot e^{-3.12i} & 1.10 \times 10^{-2} \end{pmatrix}, \quad (74)$$

$$Y_e^{h\text{SM}}(\mu_S) = \text{diag} (2.89 \times 10^{-6}, 6.10 \times 10^{-4}, 1.04 \times 10^{-2}). \quad (75)$$

These values are obtained by extrapolating to $\mu = \mu_S$ from the Yukawa matrices at the EW scale given by Eq. (32). Note that $Y^{\ell 1}$ is related to the neutrino Yukawa coupling and Majorana mass matrix. Since the neutrino masses and mixing will be explained by fitting Majorana matrix afterwards, we treat D_3 and U_ℓ as free parameters. In fact, D_3 is highly related to the Majorana scale μ_{ν_R} , and hence, we fix it so that μ_{ν_R} is to be around 10^{13} GeV. In the analysis, we use

$$D_3 = \text{diag} (1.38 \times 10^{-4}, 2.91 \times 10^{-2}, 0.504), \quad (76)$$

which is estimated by $Y^{\ell 2}$ with the RGE using the above input at $\mu = \mu_S$ and multiplying a factor of 20 to realize $\mu_{\nu_R} = \mathcal{O}(10^{13})$ GeV. Then, we observed that the maximum value of LFV observable is governed by the 3rd component of D_3 i.e. Eqs. (23), (72), and proportional to about the 4th (2nd) power for the LFV decay of a muon (the LFV decay of a meson). We also tested the case $D_3 = D_1 = \text{diag} (3.23 \times 10^{-6}, 1.99 \times 10^{-3}, 0.57)$,

motivated by the Pati-Salam symmetry [107]. The obtained result is similar to the one with Eq. (76).

Throughout the paper, we fixed $\cos\theta_d = \sin\theta_u = 0.9999$. The value of $\cos\theta_d$ is important to the fit of SM fermion masses and CKM parameters. According to the definitions of quark Yukawa couplings in Eq. (31), $\cos\theta_d \simeq 1$ is necessary so that \hat{H}_1 (\hat{H}_4) are approximately the up-type (down-type) Higgs doublet in the 2HDM. This may be required to explain the different hierarchical structures of up and down Yukawa matrices without fine-tuning in Eq. (31). In fact, when $\cos\theta_d = 0.9990$, our numerical results do not realize the CKM parameters within 10% accuracy. Such hierarchical mixing angles could be achieved by the hierarchical structure in the soft SUSY breaking terms. Note that the change in $\cos\theta_d$ does not alter the maximum size of LFV drastically since the heavy scalar Yukawa interactions are mainly controlled by the size of Yukawa couplings (D_3) and the structure of the Yukawa matrix (U_ℓ). Here, we parametrize U_ℓ as

$$U_\ell = \begin{pmatrix} \cos\theta_{12}^\nu & -\sin\theta_{12}^\nu & 0 \\ \sin\theta_{12}^\nu & \cos\theta_{12}^\nu & 0 \\ 0 & 0 & 1 \end{pmatrix} \begin{pmatrix} \cos\theta_{13}^\nu & 0 & -\sin\theta_{13}^\nu e^{-i\phi^\nu} \\ 0 & 1 & 0 \\ \sin\theta_{13}^\nu e^{i\phi^\nu} & 0 & \cos\theta_{13}^\nu \end{pmatrix} \begin{pmatrix} 1 & 0 & 0 \\ 0 & \cos\theta_{23}^\nu & -\sin\theta_{23}^\nu \\ 0 & \sin\theta_{23}^\nu & \cos\theta_{23}^\nu \end{pmatrix}. \quad (77)$$

For a given initial values of D_A , $A = 1, 2, 3, 4$ and U_Q as well as the parameter U_ℓ , the values of $D_{1,2,4}$ are fitted to explain the singular values of $Y_{u,d,e}^{hSM}$, and then U_Q is fitted to explain the CKM matrix. Note that the experimental values for quark and charged lepton masses and CKM parameters have errors, especially light quark masses, and we omit the corrections like SUSY threshold corrections in the analysis. In this sense, we do not need extremely precise fitting. However, too low accuracy will result in scattered predictions for FCNC processes, which is unphysical deviation. Therefore, the fits to singular values and CKM matrix are iterated until all the values are explained within 5% accuracy.

A.2 Benchmark

By the iterative procedure, we found a point which satisfies the hermitian condition Eq. (14) and the consistency condition with the fermion masses and mixing, Eq. (23). We will show one benchmark value at $\mu = \mu_R$, which corresponds to the cyan star in Fig. 2:

$$Y_{\text{bench}}^1 = \begin{pmatrix} 2.82 \times 10^{-6} & (1.55 \times 10^{-6}) \cdot e^{3.10i} & (1.38 \times 10^{-6}) \cdot e^{1.86i} \\ (1.55 \times 10^{-6}) \cdot e^{-3.10i} & 1.61 \times 10^{-3} & (1.63 \times 10^{-5}) \cdot e^{-3.14i} \\ (1.38 \times 10^{-6}) \cdot e^{-1.86i} & (1.63 \times 10^{-5}) \cdot e^{3.14i} & 0.569 \end{pmatrix}, \quad (78)$$

$$Y_{\text{bench}}^2 = \begin{pmatrix} 3.60 \times 10^{-5} & (7.67 \times 10^{-5}) \cdot e^{3.11i} & (7.70 \times 10^{-5}) \cdot e^{-1.28i} \\ (7.67 \times 10^{-5}) \cdot e^{-3.11i} & 3.68 \times 10^{-4} & (8.88 \times 10^{-4}) \cdot e^{3.12i} \\ (7.70 \times 10^{-5}) \cdot e^{1.28i} & (8.88 \times 10^{-4}) \cdot e^{-3.12i} & 1.84 \times 10^{-2} \end{pmatrix}, \quad (79)$$

$$Y_{\text{bench}}^{\ell 2} = \text{diag}(-2.99 \times 10^{-3}, 1.01 \times 10^{-3}, 2.48 \times 10^{-2}), \quad (80)$$

with mixing matrix U_ℓ being

$$U_{\ell, \text{bench}} = \begin{pmatrix} 0.311 & 0.121 & 0.943 \cdot e^{-0.100i} \\ 0.721 \cdot e^{0.0555i} & 0.676 \cdot e^{3.12i} & -0.152 \\ 0.619 \cdot e^{0.127i} & 0.727 \cdot e^{0.0418i} & -0.297 \end{pmatrix}. \quad (81)$$

Note that $Y_{\text{bench}}^{\ell 1}$ is changed by the structure of U_ℓ . After considering RGE effects, we obtain the following SM Yukawa matrices from above benchmark values at $\mu = \mu_S = 100$ TeV:

$$Y_u^{h_{\text{SM}}} = \begin{pmatrix} 4.99 \times 10^{-6} & (3.72 \times 10^{-6}) \cdot e^{3.11i} & (9.02 \times 10^{-7}) \cdot e^{1.88i} \\ (3.72 \times 10^{-6}) \cdot e^{-3.11i} & 2.50 \times 10^{-3} & (3.01 \times 10^{-5}) \cdot e^{3.13i} \\ (9.01 \times 10^{-7}) \cdot e^{-1.88i} & (3.02 \times 10^{-5}) \cdot e^{-3.13i} & 0.717 \end{pmatrix}, \quad (82)$$

$$Y_d^{h_{\text{SM}}} = \begin{pmatrix} 2.14 \times 10^{-5} & (4.56 \times 10^{-5}) \cdot e^{3.11i} & (4.14 \times 10^{-5}) \cdot e^{-1.28i} \\ (4.56 \times 10^{-5}) \cdot e^{-3.11i} & 2.26 \times 10^{-4} & (4.78 \times 10^{-4}) \cdot e^{3.12i} \\ (4.13 \times 10^{-5}) \cdot e^{1.28i} & (4.77 \times 10^{-4}) \cdot e^{-3.12i} & 1.10 \times 10^{-2} \end{pmatrix}, \quad (83)$$

$$Y_e^{h_{\text{SM}}} = \begin{pmatrix} 1.02 \times 10^{-4} & (2.15 \times 10^{-4}) \cdot e^{3.05i} & (3.16 \times 10^{-4}) \cdot e^{3.04i} \\ (2.08 \times 10^{-4}) \cdot e^{-3.05i} & 4.91 \times 10^{-4} & (5.82 \times 10^{-6}) \cdot e^{0.494i} \\ (2.21 \times 10^{-4}) \cdot e^{-3.04i} & (7.94 \times 10^{-6}) \cdot e^{-2.79i} & 1.04 \times 10^{-2} \end{pmatrix}. \quad (84)$$

By diagonalizing these Yukawa matrices and applying appropriate rotation for right-handed quarks to reproduce proper CKM structure, one can find that our fit procedure works to realize observed fermion masses and CKM parameters.

References

- [1] S. Iguro, Y. Muramatsu, Y. Omura and Y. Shigekami, JHEP **11** (2018) 046 [arXiv:1804.07478 [hep-ph]].
- [2] R. N. Mohapatra and J. C. Pati, Phys. Rev. D **11** (1975) 2558.
- [3] G. Senjanovic and R. N. Mohapatra, Phys. Rev. D **12** (1975) 1502.
- [4] J. Wess and B. Zumino, Phys. Lett. B **49** (1974) 52.
- [5] J. Wess and B. Zumino, Nucl. Phys. B **70** (1974) 39.
- [6] R. N. Mohapatra and G. Senjanovic, Phys. Lett. B **79** (1978), 283.
- [7] K. S. Babu and R. N. Mohapatra, Phys. Rev. D **41** (1990) 1286.
- [8] S. Chakdar, K. Ghosh, S. Nandi and S. K. Rai, Phys. Rev. D **88** (2013) no.9, 095005 [arXiv:1305.2641 [hep-ph]].

- [9] R. T. D’Agnolo and A. Hook, Phys. Lett. B **762** (2016) 421 [arXiv:1507.00336 [hep-ph]].
- [10] J. Kawamura, S. Okawa, Y. Omura and Y. Tang, JHEP **04** (2019) 162 [arXiv:1812.07004 [hep-ph]].
- [11] L. J. Hall and K. Harigaya, JHEP **10** (2018) 130 [arXiv:1803.08119 [hep-ph]].
- [12] N. Craig, I. Garcia Garcia, G. Koszegi and A. McCune, arXiv:2012.13416 [hep-ph].
- [13] N. Arkani-Hamed and S. Dimopoulos, JHEP **06** (2005) 073 [arXiv:hep-th/0405159 [hep-th]].
- [14] G. F. Giudice and A. Romanino, Nucl. Phys. B **699** (2004) 65 [erratum: Nucl. Phys. B **706** (2005) 487] [arXiv:hep-ph/0406088 [hep-ph]].
- [15] N. Arkani-Hamed, S. Dimopoulos, G. F. Giudice and A. Romanino, Nucl. Phys. B **709** (2005) 3 [arXiv:hep-ph/0409232 [hep-ph]].
- [16] J. D. Wells, Phys. Rev. D **71** (2005) 015013 [arXiv:hep-ph/0411041 [hep-ph]].
- [17] A. Albaid, M. Dine and P. Draper, JHEP **12** (2015) 046 [arXiv:1510.03392 [hep-ph]].
- [18] S. Chatrchyan *et al.* [CMS], Phys. Lett. B **716** (2012) 30 [arXiv:1207.7235 [hep-ex]].
- [19] G. Aad *et al.* [ATLAS], Phys. Lett. B **716** (2012) 1 [arXiv:1207.7214 [hep-ex]].
- [20] J. M. Frere, J. Galand, A. Le Yaouanc, L. Oliver, O. Pene and J. C. Raynal, Phys. Rev. D **46** (1992) 337
- [21] G. Barenboim, J. Bernabeu and M. Raidal, Nucl. Phys. B **478** (1996) 527 [arXiv:hep-ph/9608450 [hep-ph]].
- [22] M. E. Pospelov, Phys. Rev. D **56** (1997) 259 [arXiv:hep-ph/9611422 [hep-ph]].
- [23] P. Ball, J. M. Frere and J. Matias, Nucl. Phys. B **572** (2000) 3 [arXiv:hep-ph/9910211 [hep-ph]].
- [24] K. Kiers, J. Kolb, J. Lee, A. Soni and G. H. Wu, Phys. Rev. D **66** (2002) 095002 [arXiv:hep-ph/0205082 [hep-ph]].
- [25] Y. Zhang, H. An, X. Ji and R. N. Mohapatra, Phys. Rev. D **76** (2007) 091301 [arXiv:0704.1662 [hep-ph]].
- [26] Y. Zhang, H. An and X. d. Ji, Phys. Rev. D **78** (2008) 035006 [arXiv:0710.1454 [hep-ph]].

- [27] A. Maiezza, M. Nemevsek, F. Nesti and G. Senjanovic, Phys. Rev. D **82** (2010) 055022 [arXiv:1005.5160 [hep-ph]].
- [28] M. Blanke, A. J. Buras, K. Gemmler and T. Heidsieck, JHEP **03** (2012) 024 [arXiv:1111.5014 [hep-ph]].
- [29] E. Kou, C. D. Lü and F. S. Yu, JHEP **12** (2013) 102 [arXiv:1305.3173 [hep-ph]].
- [30] S. Bertolini, A. Maiezza and F. Nesti, Phys. Rev. D **89** (2014) no.9, 095028 [arXiv:1403.7112 [hep-ph]].
- [31] A. Maiezza, G. Senjanović and J. C. Vasquez, Phys. Rev. D **95** (2017) no.9, 095004 [arXiv:1612.09146 [hep-ph]].
- [32] P. S. Bhupal Dev, R. N. Mohapatra and Y. Zhang, Phys. Rev. D **98** (2018) no.7, 075028 [arXiv:1803.11167 [hep-ph]].
- [33] D. Borah, B. Fuks, D. Goswami and P. Poulose, Phys. Rev. D **98** (2018) no.3, 035008 [arXiv:1805.06910 [hep-ph]].
- [34] P. Ko, Y. Omura and C. Yu, Phys. Rev. D **85** (2012) 115010 [arXiv:1108.0350 [hep-ph]].
- [35] P. Ko, Y. Omura and C. Yu, JHEP **01** (2012) 147 [arXiv:1108.4005 [hep-ph]].
- [36] A. Crivellin, C. Greub and A. Kokulu, Phys. Rev. D **86** (2012) 054014 [arXiv:1206.2634 [hep-ph]].
- [37] A. Celis, M. Jung, X. Q. Li and A. Pich, JHEP **01** (2013) 054 [arXiv:1210.8443 [hep-ph]].
- [38] P. Ko, Y. Omura and C. Yu, JHEP **03** (2013) 151 [arXiv:1212.4607 [hep-ph]].
- [39] A. Crivellin, A. Kokulu and C. Greub, Phys. Rev. D **87** (2013) no.9, 094031 [arXiv:1303.5877 [hep-ph]].
- [40] L. de Lima, C. S. Machado, R. D. Matheus and L. A. F. do Prado, JHEP **11** (2015) 074 [arXiv:1501.06923 [hep-ph]].
- [41] Y. Omura, E. Senaha and K. Tobe, JHEP **05** (2015) 028 [arXiv:1502.07824 [hep-ph]].
- [42] Y. Omura, E. Senaha and K. Tobe, Phys. Rev. D **94** (2016) no.5, 055019 [arXiv:1511.08880 [hep-ph]].
- [43] J. M. Cline, Phys. Rev. D **93** (2016) no.7, 075017 [arXiv:1512.02210 [hep-ph]].

- [44] A. Crivellin, J. Heeck and P. Stoffer, *Phys. Rev. Lett.* **116** (2016) no.8, 081801 [arXiv:1507.07567 [hep-ph]].
- [45] Q. Y. Hu, X. Q. Li and Y. D. Yang, *Eur. Phys. J. C* **77** (2017) no.3, 190 [arXiv:1612.08867 [hep-ph]].
- [46] P. Ko, Y. Omura, Y. Shigekami and C. Yu, *Phys. Rev. D* **95** (2017) no.11, 115040 [arXiv:1702.08666 [hep-ph]].
- [47] S. Iguro and K. Tobe, *Nucl. Phys. B* **925** (2017) 560 [arXiv:1708.06176 [hep-ph]].
- [48] A. Arhrib, R. Benbrik, C. H. Chen, J. K. Parry, L. Rahili, S. Semlali and Q. S. Yan, arXiv:1710.05898 [hep-ph].
- [49] P. Arnan, D. Bećirević, F. Mescia and O. Sumensari, *Eur. Phys. J. C* **77** (2017) no.11, 796 [arXiv:1703.03426 [hep-ph]].
- [50] S. Iguro and Y. Omura, *JHEP* **05** (2018) 173 [arXiv:1802.01732 [hep-ph]].
- [51] L. Delle Rose, S. Khalil, S. J. D. King and S. Moretti, *Phys. Rev. D* **101** (2020) no.11, 115009 [arXiv:1903.11146 [hep-ph]].
- [52] S. Iguro and Y. Omura, *JHEP* **08** (2019) 098 [arXiv:1905.11778 [hep-ph]].
- [53] S. Iguro, Y. Omura and M. Takeuchi, *JHEP* **11** (2019) 130 [arXiv:1907.09845 [hep-ph]].
- [54] W. S. Hou and G. Kumar, *Phys. Rev. D* **102** (2020) 115017 [arXiv:2008.08469 [hep-ph]].
- [55] N. Ghosh and J. Lahiri, *Phys. Rev. D* **103** (2021) no.5, 055009 [arXiv:2010.03590 [hep-ph]].
- [56] K. S. Babu and R. N. Mohapatra, *Phys. Lett. B* **668** (2008) 404 [arXiv:0807.0481 [hep-ph]].
- [57] R. Kuchimanchi and R. N. Mohapatra, *Phys. Rev. Lett.* **75** (1995) 3989 [arXiv:hep-ph/9509256 [hep-ph]].
- [58] R. N. Mohapatra and A. Rasin, *Phys. Rev. Lett.* **76** (1996) 3490 [arXiv:hep-ph/9511391 [hep-ph]].
- [59] C. S. Aulakh, K. Benakli and G. Senjanovic, *Phys. Rev. Lett.* **79** (1997) 2188 [arXiv:hep-ph/9703434 [hep-ph]].
- [60] J. Gluza, *Acta Phys. Polon. B* **33** (2002), 1735 [arXiv:hep-ph/0201002 [hep-ph]].

- [61] J. Kersten and A. Y. Smirnov, Phys. Rev. D **76** (2007), 073005 [arXiv:0705.3221 [hep-ph]].
- [62] Z. z. Xing, Prog. Theor. Phys. Suppl. **180** (2009), 112 [arXiv:0905.3903 [hep-ph]].
- [63] X. G. He, S. Oh, J. Tandean and C. C. Wen, Phys. Rev. D **80** (2009), 073012 [arXiv:0907.1607 [hep-ph]].
- [64] R. Adhikari and A. Raychaudhuri, Phys. Rev. D **84** (2011), 033002 [arXiv:1004.5111 [hep-ph]].
- [65] A. Ibarra, E. Molinaro and S. T. Petcov, JHEP **09** (2010), 108 [arXiv:1007.2378 [hep-ph]].
- [66] A. Ibarra, E. Molinaro and S. T. Petcov, Phys. Rev. D **84** (2011), 013005 [arXiv:1103.6217 [hep-ph]].
- [67] C. G. Cely, A. Ibarra, E. Molinaro and S. T. Petcov, Phys. Lett. B **718** (2013), 957 [arXiv:1208.3654 [hep-ph]].
- [68] C. H. Lee, P. S. Bhupal Dev and R. N. Mohapatra, Phys. Rev. D **88** (2013) no.9, 093010 [arXiv:1309.0774 [hep-ph]].
- [69] J. Lopez-Pavon, E. Molinaro and S. T. Petcov, JHEP **11** (2015), 030 [arXiv:1506.05296 [hep-ph]].
- [70] A. Das and N. Okada, Phys. Lett. B **774** (2017), 32 [arXiv:1702.04668 [hep-ph]].
- [71] A. E. Cárcamo Hernández, M. González and N. A. Neill, Phys. Rev. D **101** (2020) no.3, 035005 [arXiv:1906.00978 [hep-ph]].
- [72] H. M. Lee, S. Raby, M. Ratz, G. G. Ross, R. Schieren, K. Schmidt-Hoberg and P. K. S. Vaudrevange, Phys. Lett. B **694** (2011) 491 [arXiv:1009.0905 [hep-ph]].
- [73] H. M. Lee, S. Raby, M. Ratz, G. G. Ross, R. Schieren, K. Schmidt-Hoberg and P. K. S. Vaudrevange, Nucl. Phys. B **850** (2011) 1 [arXiv:1102.3595 [hep-ph]].
- [74] K. Choi, K. S. Jeong, T. Kobayashi and K. i. Okumura, Phys. Lett. B **633** (2006) 355 [arXiv:hep-ph/0508029 [hep-ph]].
- [75] K. Choi, K. S. Jeong, T. Kobayashi and K. i. Okumura, Phys. Rev. D **75** (2007) 095012 [arXiv:hep-ph/0612258 [hep-ph]].
- [76] J. Kawamura and Y. Omura, JHEP **11** (2017) 189 [arXiv:1710.03412 [hep-ph]].
- [77] K. S. Jeong and C. B. Park, arXiv:2011.11993 [hep-ph].

- [78] J. Kawamura and S. Raby, Phys. Rev. D **103** (2021) no.1, 015002 [arXiv:2009.04582 [hep-ph]].
- [79] M. x. Luo and Y. Xiao, Phys. Rev. Lett. **90** (2003) 011601 [arXiv:hep-ph/0207271 [hep-ph]].
- [80] G. F. Giudice and A. Strumia, Nucl. Phys. B **858** (2012) 63 [arXiv:1108.6077 [hep-ph]].
- [81] E. Bagnaschi, G. F. Giudice, P. Slavich and A. Strumia, JHEP **09** (2014) 092 [arXiv:1407.4081 [hep-ph]].
- [82] M. Bona *et al.* [UTfit], Phys. Rev. Lett. **97** (2006) 151803 [arXiv:hep-ph/0605213 [hep-ph]].
- [83] M. Bona *et al.* [UTfit], JHEP **03** (2008) 049 [arXiv:0707.0636 [hep-ph]].
- [84] T. Inami and C. S. Lim, Prog. Theor. Phys. **65** (1981) 297 [erratum: Prog. Theor. Phys. **65** (1981) 1772].
- [85] A. J. Buras, S. Jager and J. Urban, Nucl. Phys. B **605** (2001) 600 [arXiv:hep-ph/0102316 [hep-ph]].
- [86] A. J. Buras and J. Girrbach, JHEP **03** (2012) 052 [arXiv:1201.1302 [hep-ph]].
- [87] J. Kawamura, S. Raby and A. Trautner, Phys. Rev. D **101** (2020) no.3, 035026 [arXiv:1911.11075 [hep-ph]].
- [88] P. A. Zyla *et al.* [Particle Data Group], PTEP **2020** (2020) no.8, 083C01
- [89] J. Brod and M. Gorbahn, Phys. Rev. Lett. **108** (2012) 121801 [arXiv:1108.2036 [hep-ph]].
- [90] A. J. Buras, M. Jamin and P. H. Weisz, Nucl. Phys. B **347** (1990) 491
- [91] J. Brod and M. Gorbahn, Phys. Rev. D **82** (2010) 094026 [arXiv:1007.0684 [hep-ph]].
- [92] S. Aoki, Y. Aoki, C. Bernard, T. Blum, G. Colangelo, M. Della Morte, S. Dürr, A. X. El Khadra, H. Fukaya and R. Horsley, *et al.* Eur. Phys. J. C **74** (2014) 2890 [arXiv:1310.8555 [hep-lat]].
- [93] S. Aoki *et al.* [Flavour Lattice Averaging Group], Eur. Phys. J. C **80** (2020) no.2, 113 [arXiv:1902.08191 [hep-lat]].
- [94] J. Urban, F. Krauss, U. Jentschura and G. Soff, Nucl. Phys. B **523** (1998) 40 [arXiv:hep-ph/9710245 [hep-ph]].

- [95] J. Aebischer, C. Bobeth, A. J. Buras, J. M. Gérard and D. M. Straub, *Phys. Lett. B* **792** (2019), 465-469 [arXiv:1807.02520 [hep-ph]].
- [96] A. K. Perrevoort [Mu3e], *EPJ Web Conf.* **118** (2016) 01028 [arXiv:1605.02906 [physics.ins-det]].
- [97] U. Bellgardt *et al.* [SINDRUM], *Nucl. Phys. B* **299** (1988) 1.
- [98] R. Kitano, M. Koike and Y. Okada, *Phys. Rev. D* **66** (2002) 096002 [erratum: *Phys. Rev. D* **76** (2007) 059902] [arXiv:hep-ph/0203110 [hep-ph]].
- [99] Y. Kuno [COMET], *PTEP* **2013** (2013) 022C01.
- [100] W. H. Bertl *et al.* [SINDRUM II], *Eur. Phys. J. C* **47** (2006) 337.
- [101] D. Ambrose *et al.* [BNL], *Phys. Rev. Lett.* **81** (1998) 5734 [arXiv:hep-ex/9811038 [hep-ex]].
- [102] R. Aaij *et al.* [LHCb], *Phys. Lett. B* **754** (2016) 167 [arXiv:1512.00322 [hep-ex]].
- [103] R. Aaij *et al.* [LHCb], *JHEP* **03** (2018) 078 [arXiv:1710.04111 [hep-ex]].
- [104] B. Aubert *et al.* [BaBar], *Phys. Rev. D* **77** (2008) 091104 [arXiv:0801.0697 [hep-ex]].
- [105] R. Aaij *et al.* [LHCb], *Phys. Rev. Lett.* **123** (2019) no.21, 211801 [arXiv:1905.06614 [hep-ex]].
- [106] M. Borsato, V. V. Gligorov, D. Guadagnoli, D. Martinez Santos and O. Sumensari, *Phys. Rev. D* **99** (2019) no.5, 055017 [arXiv:1808.02006 [hep-ph]].
- [107] J. C. Pati and A. Salam, *Phys. Rev. D* **10** (1974) 275 [erratum: *Phys. Rev. D* **11** (1975) 703].